On the Feasibility and Suitability of MR Fluid Clutches in Human-Friendly Manipulators

Article *in* IEEE/ASME Transactions on Mechatronics · January 2012

DOI: 10.1109/TMECH.2010.2074210 · Source: IEEE Xplore

2 authors, including:

Mehrdad R. Kermani
The University of Western Ontario

On the Feasibility and Suitability of MR Fluid Clutches in Human-Friendly Manipulators

Alex S. Shafer and Mehrdad R. Kermani, *Member, IEEE*

***Abstract*—An investigation into the suitability of magneto-rheological (MR) clutches in the context of developing feasible actuation solutions for physical human–robot interaction is presented. Contact and collision forces pose great danger to humans, and thus, the primary criteria for actuator development is safety. While the majority of existing solutions make use of mechanical compliance in some form, in this paper, we will approach the problem by considering the use of MR clutches for coupling the motor drive to the joint. The suitability of MR actuators to provide an intrinsically safe actuation platform is investigated by modeling the torque to mass, and torque to inertia ratios, as well as output impedance of the MR clutch. These figures are compared to commercially available servo motors as well as mechanically compliant based human-safe actuator models. The MR clutch is analytically shown to have superior mass and inertia characteristics over servo motors while either matching or surpassing the intrinsic safety characteristics of the modeled compliant actuator. The implementation of MR-clutch-based actuation systems is investigated by examining the distributed active semiactive approach. The proposed approach is discussed in terms of mechanical as well controller complexity and relates the investigation to the feasibility of practical implementations. Performance characteristics are empirically investigated by experimentation with a prototype MR clutch constructed for this purpose. The prototype MR clutch can transmit torque up to 75 Nm and has a bandwidth of 30 Hz. Torque to mass and torque to inertia ratios of the prototype MR clutch are substantially greater than that of comparable servo motors. Conclusions drawn from this investigation indicate that indeed MR clutch actuation approaches can be developed to balance safety and performance while maintaining reasonable system complexity.**

***Index Terms*—Human–robot interaction, magneto-rheological (MR) fluids, safety and performance.**

I. Introduction

INCREASINGLY, we are witnessing a growing number of developments in the field of robotics characterized by their intent to integrate man and machine in a safe and functional manner [1]–[3]. The suitability of a manipulator to work in close proximity with humans is determined first by the level of safety it can guarantee toward its human counterparts. Guaranteeing safety is a difficult if not impossible exercise as we can rarely guarantee the dependability of the numerous components required to complete a modern manipulator. Add in the human factor, and our task becomes insurmountable. Thus, much focus has been centered on interactive robots that are expected to perform in a safe and dependable manner in unknown and unpredictable environments. Collisions between robots and humans constitute the primary safety concern. Such collisions are responsible for numerous injuries each year [4], despite the existence of barriers and other fail-safe mechanisms. As we move closer toward a shared environment, new approaches to manipulator design are becoming increasingly important. Devices utilizing the unique properties of magneto-rheological (MR) fluids have been developed for robotic applications, however, almost entirely for use in haptic systems [5]–[9]. While it has been suggested in the literature how such devices might be used in a manipulator to improve both safety and performance (i.e., [10], [11]), there appears to be a general reluctance toward adopting such technology as a viable alternative to the current solutions.

Control design and software issues for the manipulators intended to interact with humans also present a set of unique challenges [12]. It is necessary to address safety, not only at the design, but at motion planning and control levels as well. Of high importance are identification and assessment of various sources of danger [13]–[16] as well as obtaining simple but realistic models of the environment and in particular of humans [17], [18]. It is however, beyond the scope of this paper to adequately discuss all subject matters. For more comprehensive review of the software issues see [19].

This paper is organized in seven sections. Section II briefly discusses fundamental issues relating to actuator and manipulator design that have detrimental effects on safety, as well as review the shortcomings of existing solutions. Section III reviews the construction and principles of the MR clutch, used to develop MR actuators (MRAs). Section IV presents an investigation into MR clutch actuators' figures of merit to provide a comparison to differing actuator types. In Section V, we propose an elaborated MR-based actuation approach that leverages the strengths highlighted in the previous section. The goals of the proposed actuation approach are to maintain safe physical interactions with humans, while improving the performance over existing human-safe actuation techniques. Section VI highlights the results of performance validation experiments conducted on a prototype MRA. Finally, concluding remarks are given in Section VII.

Manuscript received March 24, 2010; revised July 2, 2010; accepted July 17, 2010. Recommended by Technical Editor M. O'Malley.

A. S. Shafer is with the Department of Electrical and Computer Engineering, University of Western Ontario, London, ON N6A 5B9, Canada (e-mail: ashafer2@uwo.ca).

M. R. Kermani is with the Department of Electrical and Computer Engineering, University of Western Ontario, London, ON N6A 5B9, Canada, and also with the Canadian Surgical Technologies and Advanced Robotics (CSTAR) Research Centre, London Health Sciences Centre, London, ON N6A 5A5, Canada. (e-mail: mkermani@eng.uwo.ca).

Q1

Color versions of one or more of the figures in this paper are available online at http://ieeexplore.ieee.org.

Digital Object Identifier 10.1109/TMECH.2010.2074210

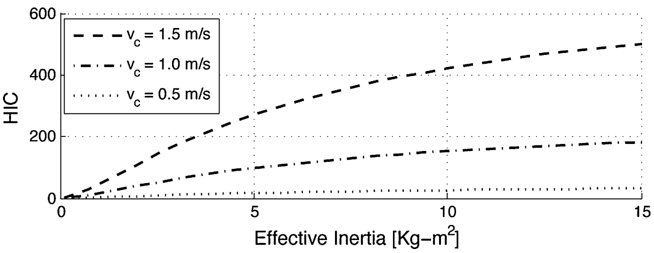

Fig. 1. Simulated HIC of a single-axis manipulator. The simulated link is rigidly coupled to the input drive. Here, V_c is collision velocity.

II. Human-Friendly Manipulators: Background and Analysis

In attempts to guarantee the safety of humans within a shared workspace, much research has been focused on the development of manipulators which are intrinsically safe. That is, manipulators which by means of their mechanical properties can guarantee some level of collision safety in the absence of a controller. To understand the degree of safety one might associate with a manipulator, we may look at the results of an uncontrolled collision through the use of the head injury criterion (HIC) [20]. The HIC along with its variations have long been used by the automotive industry to gauge the severity of collisions. In the field of robotics, it can also be used to gain similar insight. The HIC is defined as

$$\mathrm{HIC} = \max_{t_1, t_2} \left\{ (t_2 - t_1) \left(\frac{1}{t_2 - t_1} \int_{t_1}^{t_2} a(t) dt \right)^{2.5} \right\} \quad (1)$$

where a is the acceleration of the head (in g's), and t_1 and t_2 are times within the collision selected to maximize the HIC, such that $t_1 < t_2$. An HIC of 100 is the maximum value considered to be nonlife threatening. To gauge how the effective inertia of a link is related to a manipulator's inherent ability to collide safely, we simulate a single-axis robot colliding with a human head (see Fig. 1). As we may have expected, the results of the HIC indicate that a manipulator's safety can be improved by reducing its effective inertia. Thus, a generation of light-weight manipulators was inspired. One of the first manipulators to be designed under the light-weight paradigm was the whole arm manipulator (WAM) [21]. The WAM uses steel cable transmission allowing actuators to be located at the manipulator's base. Another successful implementation is the DLR-III [22]. Using light-weight carbon composites to form its links as well as advanced actuator design integrated with low-weight harmonic reduction gears, allows the DLR-III to attain a fully integrated light-weight design. These approaches however address only half of the problem. Robotic manipulators make use of high-performance servo motors to drive their links. These servo motors produce low output torque, and at high velocity with respect to what is suitable for most robots. To remedy this, gear-reduction systems are most commonly employed. The resulting torque at the link is the actuator torque multiplied by the gear ratio G_r, while the reflected actuator inertia associated with the rotor of the motor is multiplied by G_r^2. Thus, the effective inertia experienced by a robotic link can be expressed as

$$J_e = J_\ell + G_r^2 J_r \quad (2)$$

where J_ℓ is the inertia of the link, and J_r is the rotor inertia of the motor. The reflected actuator inertia of a manipulator can in fact be much larger than that of the link [23], thereby contributing a larger share of the inertial load during collisions. In response to this, several novel actuation systems have been proposed which work to decouple the reflected actuator inertia from the link. Receiving considerable attention are actuation systems that introduce compliance into their transmission. series elastic actuator (SEA) [24] accomplishes precisely this by integrating an elastic element between the motor and link. Intuitively, lower coupling stiffness results in collisions producing lower HIC values. The addition of the elastic element however dramatically reduces the controllable bandwidth of the actuator [25]. The integration of SEA devices establish a trade-off between safety and performance as a function of coupling stiffness. The variable stiffness actuator (VSA) [26] was developed to address the stringent safety-performance trade-off characterized by the SEA. Like the SEA, the VSA incorporates an elastic element into its transmission. The VSA however can alter the stiffness of the transmission coupling during task execution. It can be observed from Fig. 1 that at lower velocities, collisions involving stiff manipulators may still occur safely. By dynamically varying the stiffness to be compliant for high velocities, and stiff at low velocities, performance can be improved while maintaining safety.

Chew *et al.* [27] proposed the series damper actuator (SDA) as a means of achieving force/torque control. The SDA is constructed by placing a rotary damper in series with the motor drive. Force/torque control is achieved by controlling the relative angular velocity between the motor drive and the damper output. Similar to the SEA, the SDA has inherent impact absorption properties, which are attributed to the dissipative nature of the series damper. Similarly to the addition of an elastic element, the SDA reduces the actuator bandwidth for decreasing coupling viscosity. Again, a trade-off exists between safety and performance, in this case parameterized by the damping coefficient. (It should be noted that the authors of [27] suggest how MR fluids can be used to vary the damping coefficient). Using a damping element over an elastic element subsequently reduces the order of the system by one. This implies that the SDA is capable of achieving a larger force bandwidth over the SEA.

Variable impedance actuation (VIA) [28] combines both variable elastic and variable damping elements in the transmission. This approach is an extension of the VSA concept. By being able to vary both an elastic and a damping element, it is possible to again recuperate performance during task execution while guaranteeing the safety of humans. The VIA further requires additional actuators to vary coupling parameters.

Another notable variation on the SEA is the distributed macro-mini actuation approach (DM^2) [23]. Actuation of the joint is achieved by the coupling of a low-frequency high-torque SEA with a high-frequency low-torque servo. The high-frequency servo, directly coupled to the joint, is used to actuate the manipulator in a complimentary frequency space to that of the

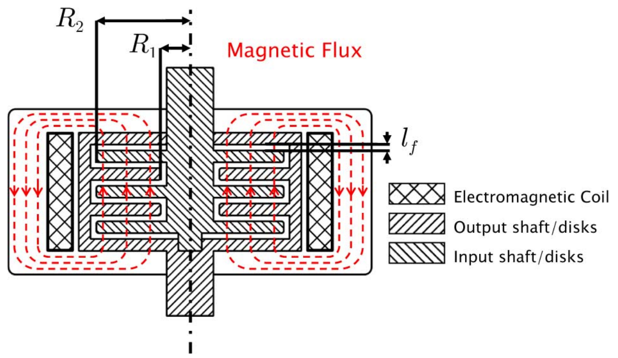

Fig. 2. Cross section of a multidisk style MR clutch and its corresponding magnetic circuit.

SEA. In this way, the effective controllable bandwidth of the manipulator is improved. The low-torque high-frequency servo is selected such that its output inertia is minimized. Thus, safety is maintained while performance is improved.

III. MR Clutch

MR fluids are a suspension of micrometer-sized particles in a carrier fluid. When subjected to a magnetic field, the particles aggregate into columns aligned in the direction of the field. Subsequently, the columns act to resist shearing of the fluid perpendicular to the field. The apparent yield stress of the fluid is dependant on, and increases with the intensity of the applied field.

Fig. 2 is a cross section of a multidisk style MR fluid clutch. MR fluid fills the volume between input and output disks. Rotation of the input shaft causes shearing in the fluid with respect to the output shaft. By energizing the electromagnetic coil, a field is induced in the MR fluid altering its apparent viscosity. The outer casing of the MR clutch acts as the magnetic flux path required to complete the magnetic circuit. The Bingham viscoplastic model is commonly used to represent the shear stress of the fluid as a function of the applied field and shear rate [29]. The model is given by

$$\tau = \tau_y(\mathbf{H}) + \eta \frac{dv}{dz}, \qquad \tau > \tau_y \tag{3}$$

where τ is the shear stress, τ_y is the field-dependant yield stress, $\mathbf{H}$ is the applied magnetic field intensity, η is the newtonian viscosity, and dv/dz is the velocity gradient in the direction of the field. Applying the Bingham viscoplastic model to a clutch, we define r as the radius from the rotational axis, and l_f as the thickness of the fluid-filled gap between input and output disks. In situations where $r \gg l_f$ for $r \in [R_1, R_2]$ (see to Fig. 2), the velocity gradient becomes constant. We can then rewrite (3) as

$$\tau = \tau_y(\mathbf{H}) + \eta\dot{\gamma}(r), \qquad \tau > \tau_y \tag{4}$$

where the shear rate $\dot{\gamma}$ is defined as

$$\dot{\gamma} = \frac{\omega r}{l_f} \tag{5}$$

and ω is the angular velocity between input and output shafts of the clutch. The torque produced by a circumferential element at a radius r is given by

$$dT = 2\pi r^2 \tau dr. \tag{6}$$

We define a clutch as having N output disks. Substituting (4) into (6) and integrating across both faces of each output disk, we arrive at

$$\begin{aligned} T &= 2N \int_{R_1}^{R_2} 2\pi \left(\tau_y(\mathbf{H}) r^2 + \eta \frac{\omega r^3}{l_f} \right) dr \\ &= 4N\pi \left(\frac{\tau_y(\mathbf{H})(R_2^3 - R_1^3)}{3} + \frac{\eta\omega(R_2^4 - R_1^4)}{4 l_f} \right) \end{aligned} \tag{7}$$

as the torque transmitted by an N-disk clutch. Data relating the yield stress τ_y of a fluid to an applied field are generally published by the manufacturer. The viscosity η of the carrier fluid is typically in the range of 0.1–0.3 Pas. The maximum torque transmission capability of an MR clutch is dependent on the maximum yield stress the material can produce. MR fluids exhibit saturation in their yield stress at high field strengths. This is a result of the underlying physics, and limits the amount of torque a particular MR fluid can transmit in clutch applications. MR fluids can produce maximum yield stresses typically in the range of 50–100 kPa [30] depending on their chemistry. MR fluids respond to an applied field on the order of 1 ms. However, the actuation response of an MR clutch becomes delayed due to field propagation through the magnetic circuit [31].

IV. MR Clutch Actuators: Investigating Figures of Merit

In Section II, we discussed the effects of actuator mass, output inertia, and output impedance on safety. In this section, we will present models relating torque to mass, torque to inertia, as well as the output impedance of (MRA).

Several configurations exist in which MR clutches can be utilized to develop an actuation system. The simplest configuration utilizes a motor to drive an MR clutch, which in turn drives the joint. To generalize the discussion, we will consider simplified mechanical models of the MR clutch based on the model presented in Section III. Note that in this section, we define the actuator output to be the output of an MR clutch.

A. Actuator Inertia

MRAs have the characteristic of replacing the reflected rotor inertia of the motor with the reflected inertia of the clutch output shaft and disks. The benefit of MRAs is their high torque to output inertia ratio as compared to servo motors. To show this, we approximate the radius of the output shaft to be equivalent to R_1. The moment of inertia of a single output disk, J_d is given by

$$J_d = \frac{1}{2}\pi \rho_d l_d \left(R_2^4 - R_1^4\right) \tag{8}$$

where ρ_d is the mass density of the disk material, l_d is the thickness of the disk (commonly between 0.5 to 1 mm), and R_1 and R_2 define the minor and major radii, respectively, of the output disk. If we consider the torque transmitted solely by the field-dependant yield stress of the MR fluid, the torque transmission of a single disk is then given by

$$T_d = \frac{4}{3}\pi\tau_y\left(R_2^3 - R_1^3\right). \tag{9}$$

Furthermore, if we consider R_1 to be small, i.e., $R_2 \gg R_1$, then the contribution of the shaft region to both (8) and (9) is also small. By allowing R_1 to equal zero, we can approximate the torque–inertia ratio of a single disk to be

$$\alpha = \frac{T_d}{J_d} = \frac{8}{3}\frac{\tau_y}{\rho_d l_d R_2}. \tag{10}$$

As observed, the ratio becomes less favorable as R_2 increases. This however is not the final measure that dictates the actuators suitability. To grasp the overall effects of increasing radius, and hence, torque capacity, the reflected inertia at the joint should be consider. The reason for this is that as radius increases along with torque capacity, the gear ratio required to amplify the actuator's torque decreases. As the actuator inertia multiplies the square of the gear ratio to arrive at the reflected inertia at the joint, the analysis becomes important. The reflected inertia of the MR clutch at the manipulator joint is given by

$$J_c' = \frac{1}{2}\pi\rho_d l_d N\left(R_2^4 - R_1^4\right)G_r^2 \tag{11}$$

where we have included N to multiply the inertia by the number of disks in the clutch. The gear ratio G_r is defined as

$$G_r = \frac{T_c'}{T_c} \tag{12}$$

where T_c' is the desired torque at the joint, and T_c is the output torque of the clutch. Rearranging (9) to show the outer radius R_2 as a function of the clutch output torque yields

$$R_2 = \left(\frac{3}{4}\frac{T_c}{\pi\tau_y N} + R_1^3\right)^{1/3}. \tag{13}$$

We can then write (13) representing the reflected inertia of a MR clutch at the manipulator joint as a function of the clutch torque

$$J_c' = \frac{1}{2}\pi\rho_d l_d N\left(\left(\frac{3}{4}\frac{T_c}{\pi\tau_y N} + R_1^3\right)^{4/3} - R_1^4\right)\left(\frac{T_c'}{T_c}\right)^2. \tag{14}$$

Fig. 3 shows the values of reflected actuator inertia versus output torque for the MR clutch. The plot also includes equivalent values for commercially available low-inertia servo motors. It is evident that the MR clutch demonstrates superior output inertia characteristics over the low-inertia servo motors. We note that the developed torque to inertia relationship improves dramatically at larger values of output torque.

B. Mass of MR Clutch

In this section, we develop torque to mass relationships for the MR clutch. While the relationships are developed using simplified geometric models, they serve to establish the order in which the clutch mass compares to that of servo motors, as well as the rate at which clutch mass increases with respect to transmittable torque capacity. To develop a relationship between clutch mass and torque capacity for MR fluid clutches, we consider the simplified geometric model detailed in Fig. 4. We will solve for required parametric values through the application of magnetic circuit analysis. We divide the reluctance of the core $\Re_c$ into three sections, namely $\Re_{c_1}$, $\Re_{c_2}$, and $\Re_{c_3}$. The symmetric geometry of the model dictates the reluctance $\Re_{c_2}$ to be equivalent to that of $\Re_{c_3}$. Thus, we define the reluctance of the core to be

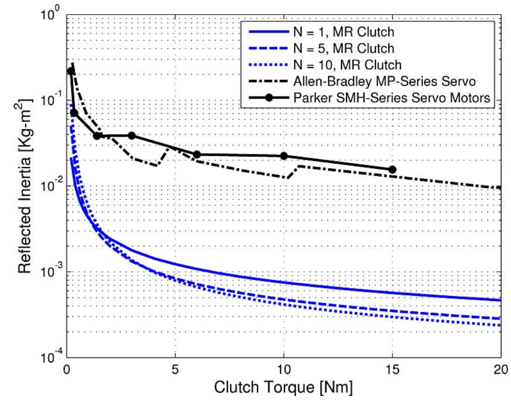

Fig. 3. Reflected inertia versus output torque for the MR clutch (see Table I) and commercially available low-inertia servo motors. ($T_c' = 50$ Nm).

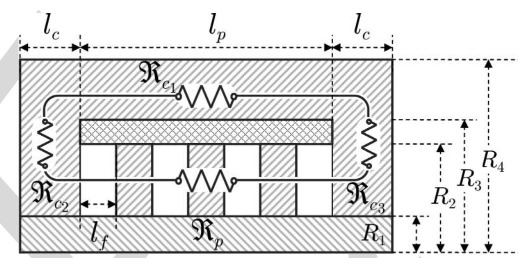

Fig. 4. Simplified MR clutch model. The electromagnetic coil is contained between R_2 and R_3, and R_4 defines the outer surface of the ferrous core.

$$\Re_c = \Re_{c_1} + 2\,\Re_{c_{23}} \tag{15}$$

where $\Re_{c_{23}} = \Re_{c_2} = \Re_{c_3}$. We have defined a clutch by the number of output disks N coupled to the output shaft. For N output disks, a clutch is required to have $N-1$ input disks, and a total of $2N$ MR fluid interface gaps positioned between input and output disks. In the simplified model of Fig. 4, we define both geometric and material properties of the input and output disks to be identical. The disk pack assembly thus contains $2N-1$ disks and $2N$ MR fluid interface gaps. The reluctance of the disk pack assembly $\Re_p$ can then be written as

$$\Re_p = (2N-1)\,\Re_d + 2N\,\Re_f \tag{16}$$

where $\Re_d$ and $\Re_f$ are the reluctance of a single disk and single MR fluid interface gap, respectively. The reluctance of a material is given by $\Re = l/(\mu_0\mu_r A)$, where l is the mean length of the flux path through the material, $\mu_0 = 4\pi \times 10^{-7}$ H/m is the permeability of free space, μ_r is the relative permeability of the material, and A is the cross-sectional area of the material perpendicular to the flux path. Assuming that the mean flux path through any of the circuit members lies at its geometric center,

TABLE I
PARAMETER VALUES FOR SIMPLIFIED MR CLUTCH MODEL

Parameter	Symbol	Value
Disk thickness	l_d	1.0 [mm]
Fluid gap thickness	l_f	0.5 [mm]
Disk minor radius	R_1	10 [mm]
Max operating yield stress	τ_y^*	40 [kpa]
Coil current density	J_w	2.5 $\times 10^6$ [A/m^2]

we can then derive the reluctance of the individual components of the simplified clutch model to be

$$\Re_{c_1} = \frac{l_p + l_c}{\mu_0 \mu_{r_s} \, \pi \left(R_4^2 - R_3^2\right)}$$
$$\Re_{c_{23}} = \int_{R_2 + R_1/2}^{R_4 + R_3/2} \frac{dr}{\mu_0 \mu_{r_s} \, (2\pi r) \, l_c} = \frac{\ln \left(R_4 + R_3/R_2 + R_1\right)}{2\mu_0 \mu_{r_s} \, \pi l_c}$$
$$\Re_d = \frac{l_d}{\mu_0 \mu_{r_s} \, \pi \left(R_2^2 - R_1^2\right)} \quad \Re_f = \frac{l_f}{\mu_0 \mu_{r_f} \, \pi \left(R_2^2 - R_1^2\right)}. \tag{17}$$

Here, μ_{r_s} is the permeability of steel, the material used for both the core and disks, μ_{r_f} is the permeability of the MR fluid, l_d is the thickness of a single disk, l_f is the distance between input and output disks forming the MR fluid gap, l_c is the thickness of the equivalent core sections, and $l_p = (2N - 1)\, l_d + 2N l_f$ is the length of the disk pack. The flux ϕ in the circuit is then given by

$$\phi = \frac{I}{\Re_c + \Re_p} = \frac{l_p (R_3 - R_2) J_w}{\Re_c + \Re_p} \tag{18}$$

where I is the total electric current through the cross section of the magnetic coil, and J_w is the current density of the coil cross section. The magnetic field intensity $\mathbf{H}$ at any point within the circuit is related to the circuit flux ϕ by

$$\mathbf{H} = \frac{\phi}{\mu_0 \mu_r A} \tag{19}$$

where again, μ_r and A are, respectively, the relative permeability and cross sectional area of the material at which the magnetic-field intensity $\mathbf{H}$ is to be determined. We now define the parameter τ_y^* as the maximum yield stress at which the MR fluid is to operate. Using data provided by the MR fluid manufacturer relating the yield stress of the fluid to the applied magnetic field, we define $\mathbf{H}^*$ as the magnetic-field intensity in the MR fluid required to produce the yield stress τ_y^*. Rearranging (19), and substituting the appropriate MR fluid geometric and material values, we define ϕ^* as the flux required in the circuit to produce $\mathbf{H}^*$ in the MR fluid

$$\phi^* = \mu_0 \mu_{r_f} \, \pi \left(R_2^2 - R_1^2\right) \mathbf{H}^*. \tag{20}$$

R_2 is uniquely defined by the parameters T_c, N, R_1, and τ_y^* [refer to (13)]. Thus, for the given set of fixed parameters given in Table I, we solve for the values of R_3, R_4, and l_c that satisfy (18) for $\phi = \phi^*$, while simultaneously minimizing the clutch mass m_{MRC} given by

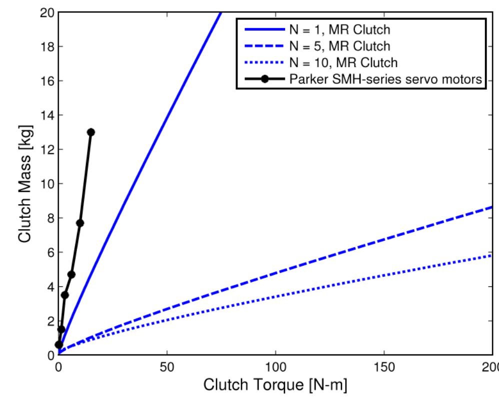

Fig. 5. Mass of simplified clutch models versus torque capacity (calculated using MR fluid characteristics of Lord Corp., MR-132DG MR fluid [32]).

$$\begin{aligned} m_{\text{MRC}} &= m_c + m_p + m_s + m_w \\ m_c &= \pi \left[\left(R_4^2 - R_3^2\right) l_p + 2 \left(R_4^2 - R_1^2\right) l_c \right] \rho_s \\ m_p &= \pi \left[(2N - 1)\, l_d \rho_s + 2N l_f \rho_f \right] \left(R_2^2 - R_1^2\right) \\ m_w &= \pi \left(R_3^2 - R_2^2\right) l_p \rho_{\text{cu}} \qquad m_s = \pi R_1^2 \left(l_p + 2\, l_c\right) \rho_{\text{al}} \end{aligned} \tag{21}$$

where m_c is the mass of the core, m_p is the mass of the disk pack assembly which includes the MR fluid, m_s is the mass of the shaft, and m_w is the mass of the magnetic coil. In (21), ρ_s, ρ_f, ρ_{cu}, and ρ_{al} are the mass densities of steel, MR fluid, copper, and aluminum, respectively. Fig. 5 shows the torque to mass relationship of the simplified MR clutch model and compares it to a commercially available servo motor. We note that due to the mass overhead associated with the material required to form the magnetic circuit, the torque to mass ratio of the MR clutch is less favorable at very low values N. In the developed model, we observe superior characteristics over the commercially available servo motor.

C. Output Impedance

The output impedance of an actuator can be defined as

$$Z(s) = \frac{F_l(s)}{X_l(s)} \tag{22}$$

where $F_l(s)$ is the force experienced by the load and $X_l(s)$ is the displacement of the load. Actuators that limit or reduce their impedance, especially at higher frequencies, offer a higher degree of safety over those that do not. Within the controllable bandwidth, impedance can be actively reduced by control action. However, above the controllable bandwidth, the impedance is dominated by the open-loop characteristics of the actuator and link. To form a comparison of the intrinsic properties of human safe actuators, we consider the output impedance in the absence of control. This is intended to represent the open-loop characteristics resulting from collisions occurring above the control bandwidth. Fig. 6 shows a schematic representation of the MRA and SEA models under consideration here. In this scenario, both

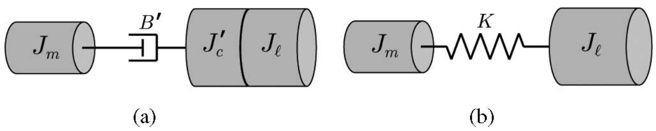

Fig. 6. Model schematic of unpowered (a) MRA, and (b) SEA.

motor and clutch are unpowered, allowing us to model the clutch as a damper and inertial load. J_m is the inertia of the motor for both the MRA and SEA, K is the spring constant of the SEA, B'_c is the damping coefficient of the MR clutch reflected to the link, J'_c is the output inertia of the MR clutch reflected to the link, and J_ℓ is the inertia of the link. The damping coefficient in the MR clutch is determined by the Newtonian viscosity of the MR fluid (the viscosity at zero field) as well as the clutch geometry. The output impedance of the SEA is given by

$$Z_{\mathrm{SEA}} = J_\ell s^2 + \frac{K J_m s^2}{J_m s^2 + K}. \tag{23}$$

The value of the link inertia J_ℓ for the purpose of discussing the characteristics of the SEA is somewhat arbitrary, and it is, thus, not uncommon to disregard it (allowing J_ℓ to equal zero). This results in the properties of the SEA being characterized by the second term only. In this circumstance, the output impedance approaches the value of the spring constant K at high frequencies. It is this property of the SEA to limit output impedance above the controllable bandwidth that intrinsically insures safe interaction forces as well as impact loads. The output impedance of the MRA is given as

$$Z_{\mathrm{MRA}} = (J'_c + J_\ell)\, s^2 + \frac{B'_c J_m s^2}{J_m s + B'_c}. \tag{24}$$

A fair comparison would dictate if we once more disregard the
Q3 link inertia J_ℓ. While the second term increases (approximately) proportional to the reflected damping coefficient B'_c, at higher frequencies it is the reflected inertia of the clutch J'_c in the first term that dominates the dynamics of the output impedance. Noting that the output impedance of the MRA is not limited, but rather continues to grow at high frequencies, seemingly, it would not appear that the MRA poses the intrinsic safety characteristics of the SEA. However, to fairly evaluate the deficiency of the MRA in this respect, it is instructive to consider practical examples to establish the context in which the SEA offers superior safety. If we reconsider the actuator models to include the inertia of the link, for both the SEA and MRA, the inertial impedance represented in the first terms will dominate the output impedances at higher frequencies. The output impedance of the MRA can thus approach that of the SEA if $J'_c \ll J_\ell$. To demonstrate the conditions in which we can satisfy $J'_c \ll J_\ell$, we consider an applications requiring 50 Nm at the link. From the values presented in Fig. 3, we can expect that the reflected inertia of an MRA satisfying the 50-Nm requirement, would be on the order of 10^{-3} kg m^2. We may then prescribe a lower bound link inertia on the order of $J_\ell = 10^{-2}$ kg m^2, and one order of magnitude larger than J'_c, the result of which being that $(J_\ell + J'_c) \approx J_\ell$. To put the values into perspective, we can express this lower bound as a link modeled by a point mass of

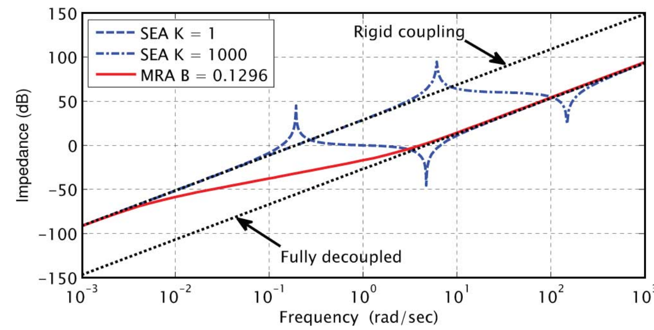

Fig. 7. Simulated output impedance for SEA and MRA. Values obtained from experimental MRA setup: $J_m = 26.9$ kg m^2; $J'_c = 5 \times 10^{-3}$ kg m^2; $J_\ell = 0.045$ kg m^2; $B = 0.1296$ Ns m^{-1}. MRA produces 75-Nm output.

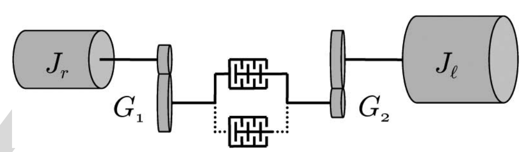

Fig. 8. DASA: solid line represents single clutch configuration, dotted line represents connection to second clutch present only in antagonistic configuration.

250 g at a radius of 20 cm. Links having inertias above this lower bound could then be driven by either MRA or SEA and exhibit nearly identical inertial impedances. In the application region of 50 Nm, it is reasonable to expect that most links will have inertias larger than our defined lower bound. The implication being that an SEA would not provide a safety improvement over an MRA in the stated application region. It must be pointed out that we have assumed the values presented in Fig. 3, which have been computed from idealized models, are realistically achievable. Fig. 7 shows simulated output impedances for both an MRA and SEA. Values for the motor, MR clutch, and link inertias, as well as clutch damping coefficient were obtained from an experimental MRA setup (discussed later in greater detail). Using these values, the output impedance of the MRA is simulated and compared to that of an SEA. We see that in this circumstance, the MRA demonstrates superior output impedance characteristics over that of the SEA. This is complimented by the superior performance provided by the MRA.

V. Distributed Active SemiActive Actuation

In this section, we propose an actuation technique that leverages the unique properties of MRAs. The proposed technique is unique in which we attempt to reconcile safety, performance, and complexity into a feasible solution. The distributed active semiactive (DASA) actuation approach locates a driving motor (the active actuator) at the base of the robot, and a semiactive MR clutch at the joint (see to Fig. 8). The gear ratios G_1 and G_2 are balanced to give the desired mass, and reflected output inertia at the link. Reducing G_1 reduces the requirements of the clutch transmission torque, which thus reduces the mass of the clutch, however, the reflected output inertia is inevitably increased as G_2 must then be increased to compensate. In Section IV, we have shown how actuating a joint via an MR clutch can reduce mass and reflected output inertia over conventional servo motors. The impact on safety is immediately appreciated as the effective inertia of the link is instantly reduced. This not only improves manipulator performance, but further allows a manipulator to operate at higher velocities while maintaining safe HIC values in the event of a collision. Moreover, the clutch itself is back drivable, and can be thought of as exhibiting the properties of an ideal torque source. This is an important characteristic for human-friendly actuators as it facilitates impedance control. While motors themselves are also intrinsically back drivable, the high-ratio-gear reductions they require are often not. Thus, highly performing low-weight robots, which implement low mass motors at the expense of high-ratio-gear reductions rely on torque sensors in the control loop to electronically implement back-drivable behavior. MR clutches posses a superior torque to mass ratios over their servo motor counterparts, and thus can be designed to require much lower reduction ratios, if not developed as direct-drive components, either way retaining their intrinsic back-drivability. MR clutches have the added benefit of uniform torque transmission independent of armature position, unlike servo motors, which suffer from nonlinearities such as cogging torque. Relocating the driving motor to the base of a robot in order to reduce the mass at the link is not a new concept. However, it has been a restrictive practice as the newly required transmission responsible for bringing mechanical power from the base to the joint has commonly introduced unwanted friction and compliance, which have reduced performance, and complicated the control system. The DASA implementation however can be controlled to operate in a region in which torque transmission is relatively immune to perturbation in the relative angular velocity ω within the clutch, effectively allowing the clutch to act as a mechanical power filter. This characteristic which will be explained momentarily allows the DASA system to function with less than ideal mechanical transmission while maintaining the performance and characteristics of a "stiff" transmission at the joint. To explain this, we consider that the the Bingham model is accurate for describing the rheology of the fluid for shear stress τ above the field-dependant yield stress τ_y, as expressed in (3). It is this "Bingham region" in which we wish the clutch to operate in order to benefit from the aforementioned characteristics. Below the yield stress τ_y, however, the fluid exhibits newtonian characteristics, i.e., to say that τ grows with a nonnegligible proportionality to the shear rate $\dot{\gamma}$ (for a more in-depth analysis see [33]). We can thus attribute a field-dependant shear rate threshold $\dot{\gamma}^*$ below, which the fluid exhibits newtonian characteristics, and above which, the Bingham model applies. To maintain the clutch in the Bingham region, the fluid at any radius r within the clutch must maintain a shear rate above $\dot{\gamma}^*$. To guarantee this condition, we define the field-dependant angular velocity ω^*, the threshold above which operation in the Bingham region is ensured as

$$\omega^* = \frac{\dot{\gamma}^* l_f}{R_1}. \tag{25}$$

We come to (25) by rearranging (5) and substituting r with its minimum value R_1, the critical radius at which the lowest shear rate $\dot{\gamma}$ occurs. The control strategy should therefore attempt to avoid entering the Newtonian region by controlling the motor angular velocity ω_m to satisfy the condition

$$|\omega_m| = |\omega_j - \omega^*| + \epsilon^* \tag{26}$$

where ω_j is the angular velocity of the joint, and ϵ^* is a field-dependant error margin selected to ensure that the dynamics of the motor have enough time to react to quickly varying values of ω_j. ϵ^* must be large enough to ensure $\omega \geq \omega^*$ under all dynamic situations, however, exact calculation of ϵ^* may be difficult as there is a reliance on empirical data associated with the dynamics of the joint/link. Care must be taken, however, to avoid unnecessary power dissipation, which for a clutch is defined as $P_d = T\omega$. Because ω tracks $\omega^* + \epsilon^*$, the value selected for ϵ^* cannot be arbitrarily large. Crossing into the Newtonian region is required to alter the direction of the torque transmitted to the link when utilizing a single clutch to implement the DASA system. As the motor must change the direction of its output rotation, the clutch torque transmission momentarily enters a dead zone. This has the potential of creating a substantial backlash effect.

A. *Antagonistic DASA*

An antagonistic configuration of the DASA system (see Fig. 8) is intended to increase performance, and rectify the shortcomings of the single-clutch DASA configuration. The motor drives the input to two clutches, however in opposite directions with respect to one another. The antagonistic output of the two clutches is coupled to the link. By energizing one of the two clutches, torque can be transmitted in either the clockwise or counterclockwise direction. Thus, the antagonistic configuration allows for torque transmission to the joint to alter direction without altering the direction of the motor output, thereby, eliminating the backlash introduced by the single-clutch DASA. Such devices have been developed with electro-rheological (ER) fluids [34]. Maintaining rotation of the motor shaft, the bandwidth of the antagonistic-DASA output is limited by charging and discharging of the magnetic field required to activate the clutch. If we label the two clutches of an antagonistic DASA assembly as $\mathcal{C}_1$ and $\mathcal{C}_2$, then the motor's angular velocity should track

$$\omega_m = \max\{|\omega_j - \omega_1^*|, |\omega_2^* - \omega_j|\} + \epsilon^* \tag{27}$$

to avoid entering the Newtonian region of operation in either clutch. ω_1^*, and ω_2^* are the angular velocity of the Bingham region thresholds for clutches $\mathcal{C}_1$ and $\mathcal{C}_2$, respectively. Note that in our convention, clutch $\mathcal{C}_2$ has its input reversed in direction with respect to clutch $\mathcal{C}_1$, i.e.,

$$\omega_1 = \omega_j - \omega_m \qquad \omega_2 = \omega_j + \omega_m. \tag{28}$$

The torque production for an antagonistic-DASA system operating in the Bingham region is then given by

$$T_{\mathrm{AD}} = T_1(\mathbf{H}_1) + T_2(\mathbf{H_2}) - \frac{2\pi\eta|\omega_j|}{l_f}\left(R_2^4 - R_1^4\right) \tag{29}$$

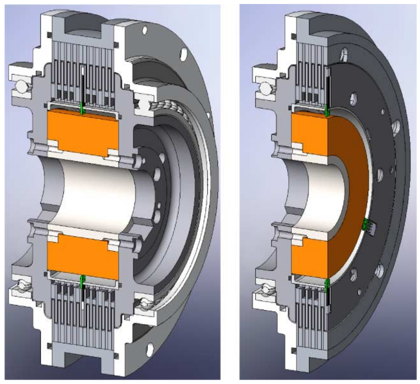

Fig. 9. Sectional views of prototype MR clutch.

where T_1 and T_2 are the field-dependant torques produced by clutches $\mathcal{C}_1$, and $\mathcal{C}_2$, respectively, given by

$$T_i = \frac{4\pi}{3}\tau_y(\mathbf{H}_i)\left(R_2^3 - R_1^3\right)\operatorname{sgn}(\omega_i), \quad i = 1, 2 \qquad (30)$$

where $\mathbf{H}_1$ and $\mathbf{H}_2$ are the fields produced in clutches $\mathcal{C}_1$, and $\mathcal{C}_2$, respectively. Note that the individual viscous torque contributions of $\mathcal{C}_1$ and $\mathcal{C}_2$ negate each other at the joint when $\omega_j = 0$. Viscosity of this class of fluids does not always obey ideal models. The antagonistic configuration can mitigate some nonlinearities which would otherwise have to be compensated for by the controller.

VI. Performance Validation of a Prototype MR Clutch

In this section, we present results obtained by experimentation with a prototype MR clutch which we have designed and constructed (see Fig. 9). The configuration of the prototype MR clutch deviates from the model of Section IV. The magnetic coil of the prototype is located radially inward of the clutch pack in a “coil-in” configuration, as opposed to the coil-out configuration previously discussed. Coupling the coil to the output shaft has the intended effect of reducing clutch mass, however comes at the expense of increasing output inertia. Design of the prototype clutch is partially automated using the optimization process discussed in Section IV-B, where model equations have been updated to reflect the change in configuration. The method returns values for the dimensional parameters that minimize the clutch mass for a given design torque. The prototype MR clutch was specified with a design torque of 120 Nm. The dimensional parameters returned by the optimization process were used as the basis for practical design. Table II compares the output torque, inertia, and mass of the physical prototype MR clutch to the optimized design model. A large discrepancy exists between the modeled and actual torque. The discrepancy results primarily due to deviations in the physical design from the geometric model used in the optimization. Practical design features required for fastening and wire access are omitted from the model. The optimization produces geometries in which flux members enter magnetic saturation at the magnitude of circuit flux corresponding to the specified design torque of the clutch. Removal of ferromagnetic material from the optimized geometry subsequently results in premature saturation of the circuit, limiting the output torque of the clutch.

TABLE II
Comparison Between Prototype and Modeled MR Clutch, as Well as Commercially Available Servomotors

	Coil-out Configuration	Prototype MR Clutch Model	Actual	Servomotors Parker SMH-100	Maxon EC60
Output Torque[Nm]	75	120	75	6.0	0.83
Mass[kg]	2.8	4.7	4.5	4.7	2.5
Inertia$\times 10^3$[kg$\cdot$m^2]	0.19	2.8	5.0	0.34	0.083
Reflected Inertia$\times 10^3$[kg$\cdot$m^2]†	-	-	2.22	23.3	302

†Reflected torque $T_c' = 50$ Nm.

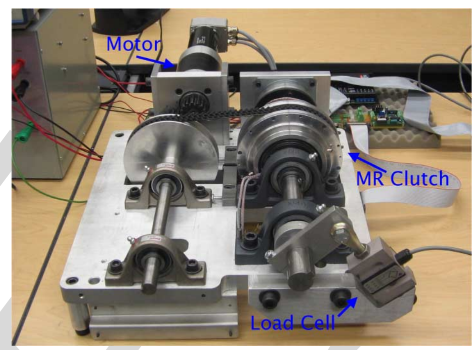

Fig. 10. Experimental setup used to verify the prototype MR clutch.

Much of our analysis prior to this section is based on the coil-out configuration model of Section IV-B. To add perspective, we compare this model to the prototype MR clutch. The values for the coil-out configuration shown in Table II are produced with the geometric model and procedure described in Section IV-B, where the output torque is specified to match the constructed MR clutch and not the design value. The coil-out model does not consider any practical design requirements, such as bearings, seals, and mechanical coupling of the disks. In this regard, the model represents an ideal scenario, or baseline for the achievable characteristics in its configuration. The comparison indicates that there is room for improvement of the prototype MR clutch. Ideally, mass could be reduced by a third, while the output inertia might be improved by an order of magnitude. Table II compares the prototype MR clutch to two commercially available servo motors. The servo motors are chosen to have comparable mass to the prototype MR clutch. The output inertia of the servo motors are between one and two orders of magnitude lower than that of the MR clutch. However, when we consider a hypothetical application requiring a 50-Nm output, the prototype MR clutch posses the more favorable reflected inertia by at least an order of magnitude.

To assess its performance characteristics, the clutch is mounted to an experimentation platform (see Fig. 10) that incorporates an angular encoder (Renishaw RM22I) to read the position of the output shaft. A static load cell (Transducer Techniques SBO-1K) mounts to the output shaft for torque experiments. A servo motor (Maxon EC 60) provides the rotational input to the MR clutch. A PID controller is implemented on a

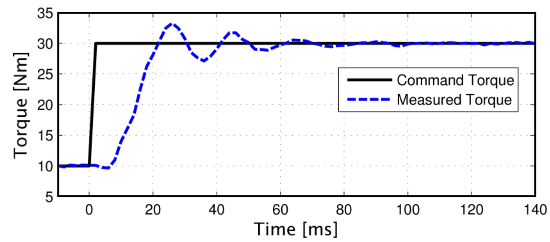

Fig. 11. Torque tracking of step reference.

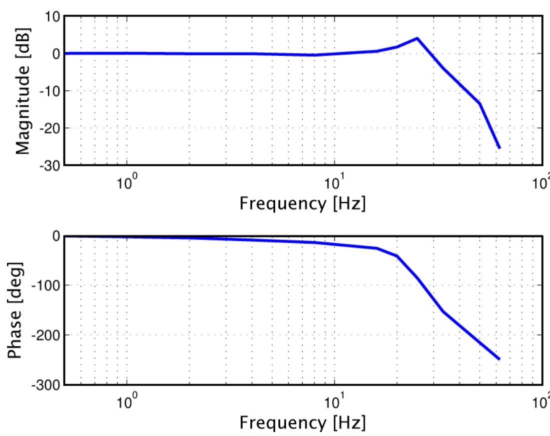

Fig. 12. Frequency response of the prototype MR clutch.

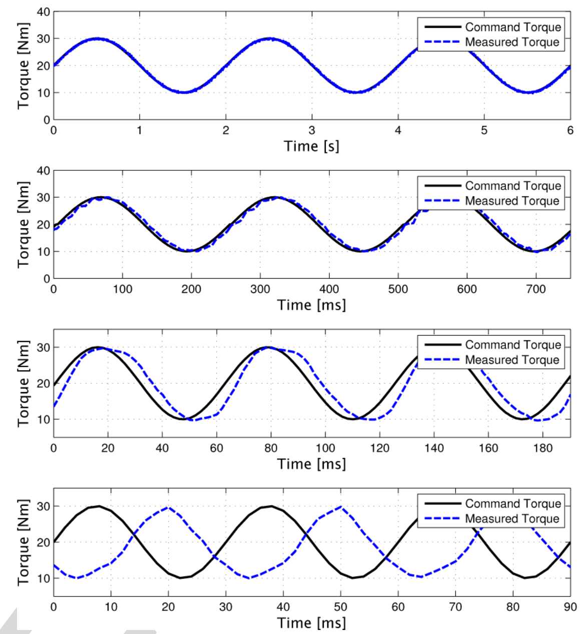

Fig. 13. Torque tracking of a sinusoidal references at frequencies of 0.5, 4.0, 16.0, and 33.3 Hz (from top to bottom).

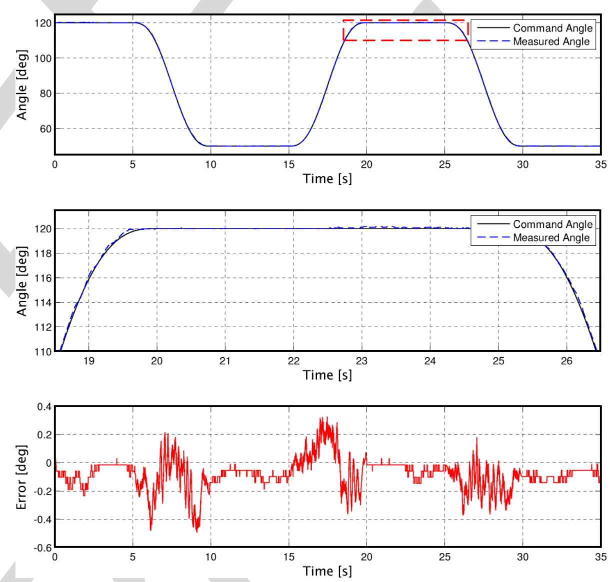

Fig. 14. Position tracking of a trajectory reference. The center plot magnifies the trajectory in the region marked by the dotted red bounding box.

desktop computer that communicates with the experimentation platform via a National Instruments (NI USB-6229) multifunction I/O device. The output signal from the PID controller forms the input signal to the current amplifier of the MR clutch, while the rotational velocity of the motor is kept constant.

Fig. 11 shows the closed-loop response to a step input. The rise time is determined to be approximately 10 ms. The frequency response and dynamic characteristics are examined by measuring the torque response to a sinusoidal reference signal and initiating a frequency sweep at 0.5 Hz. Fig. 12 shows the frequency response of the system. The resulting 3-dB actuator bandwidth is measured to be approximately 30 Hz. Fig. 13 presents a set of four time domain measurements from the sweep. Beginning at 0.5 Hz, we note excellent overlay of the measured signal with that of the command. As the reference frequency is increased toward and above the actuator bandwidth, we note that the response remains very smooth and as well retains the shape of the command signal quite well. Clean and predictable torque outputs are an asset to the development of controls and sensorization schemes that are required to monitor and control contact forces between manipulators and humans.

Trajectory tracking experiments were conducted using the angular encoder to form the feedback signal. The motor output was held at a constant rotational velocity. A 50-cm long arm constructed of medium density plastic was coupled to the output shaft. A counter weight of approximately 2 kg was mounted to the end of arm. The results shown in Fig. 14 indicate the capacity of the MR clutch in this arrangement to achieve favorable precision in position control tasks. Small fluctuation errors in the static portions of the trajectory demonstrate the capability of the MR clutch to suppress fluctuations present in the input drive.

VII. Conclusion

MR fluids exhibit promising characteristics for applications in robotics. Specifically, they are well-suited for actuation systems developed to interact physically with humans. As we have shown, MR-clutch-based actuators demonstrate excellent torque to mass, and torque to inertia characteristics. This is especially evident for clutches having large torque capacities. This creates a niche opportunity for MR-based actuators to be developed into light-weight direct-drive (DD) systems. Light-weight

DD systems exhibit several characteristics that are sought after for human-friendly manipulators, namely: intrinsic backdrivability, low output inertia, superior performance and bandwidth, as well as high precision in the control of output torque. Furthermore, MR-based actuators can potentially reduce system complexity. Potentially, the accuracy of torque transmission models in such systems could allow for high fidelity torque control without the requirement for torque sensors at the joints. This is in contrast to the increasingly complex actuation solutions proposed to deal with physical human interaction.

REFERENCES

[1] G. Hirzinger, "Mechatronics for a new robot generation," *IEEE/ASME Trans. Mechatronics*, vol. 1, no. 2, pp. 149–157, Jun. 1996.

[2] Y. Yamada, Y. Hirasawa, S. Huang, Y. Umetani, and K. Suita, "Human-robot contact in the safeguarding space," *IEEE/ASME Trans. Mechatronics*, vol. 2, no. 4, pp. 230–236, Dec. 1997.

[3] H. Lim and K. Tanie, "Collision-tolerant control of human-friendly robot with viscoelastic trunk," *IEEE/ASME Trans. Mechatronics*, vol. 4, no. 4, pp. 417–427, Dec. 1999.

[4] Industrial Robots and Robot System Safety in *OSHA Technical Manual*, United States Department of Labor, Occupational Safety and Health Administration, 2008, ch. 4. Q6

[5] J. Blake and H. B. Gurocak, "Haptic glove with mr brakes for virtual reality," *IEEE/ASME Trans. Mechatronics*, vol. 14, no. 5, pp. 606–615, Oct. 2009.

[6] Y.-J. Nam and M.-K. Park, "A hybrid haptic device for wide-ranged force reflection and improved transparency," in *Proc. Int. Conf. Control, Autom. Syst.*, 2007, pp. 1015–1020.

[7] D. Ryu, K. Moon, S. Kang, M. Kim, and J.-B. Song, "Development of wearable haptic system for tangible studio to experience a virtual heritage alive," in *Proc. IEEE/RSJ Int. Conf. Intell. Robots. Syst.*, 2006, pp. 466–471.

[8] T. Kikuchi, K. Oda, and J. Furusho, "Simulation of clonic movement with leg-robot driven by compact mr fluid clutch," in *Proc. IEEE 11th Int. Conf. Rehabil. Robot.*, 2009, pp. 80–85.

[9] S. H. Winter and M. Bouzit, "Use of magnetorheological fluid in a force feedback glove," *IEEE Trans. Neural Syst. Rehabil. Eng.*, vol. 15, no. 1, pp. 2–8, Mar. 2007.

[10] P. Fauteux, M. Lauria, M.-A. Legault, B. Heintz, and F. Michaud, "Dual differential rheological actuator for robotic interaction tasks," in *Proc. IEEE/ASME Int. Conf. Adv. Intell. Mechatron.*, 2009, pp. 47–52.

[11] S.-S. Yoon, S. Kang, S.-J. Kim, Y.-H. Kim, M. Kim, and C.-W. Lee, "Safe arm with mr-based passive compliant joints and visco-elastic covering for service robot applications," in *Proc. IEEE/RSJ Int. Conf. Intell. Robots. Syst.*, 2003, pp. 2191–2196.

[12] J. Trafton, N. Cassimatis, M. Bugajska, and D. Brock, "Enabling effective human-robot interaction using perspective-taking in robots," *IEEE Trans. Syst. Man Cybern.*, vol. 35, no. 4, pp. 460–470, Jul. 2005.

[13] K. Ikuta and M. Nokata, "Safety evaluation method of design and control of human-care robots," *Int. J. Robot. Res.*, vol. 22, pp. 281–297, 2003.

[14] O. Brock and O. Khatib, "Elastic strips: A framework for motion generation in human environments," *Int. J. Robot. Res.*, vol. 21, pp. 1031–1053, 2002.

[15] D. Kulic and E. Croft, "Pre-collision safety strategies for human-robot interaction," *Auton. Robots*, vol. 22, pp. 149–164, 2007.

[16] N. Najmaei and M. Kermani, "Prediction-based reactive control strategy for human-robot interactions," in *Proc. IEEE Int. Conf. Robot. Autom.*, 2010, pp. 3434–3439.

[17] A. Martinez and J. Vitria, "Clustering in image space for place recognition and visual annotations for human-robot interaction," *IEEE Trans. Syst. Man Cybern.*, vol. 31, no. 5, pp. 669–682, Oct. 2001.

[18] T. Moeslund, A. Hilton, and V. Kruger, "A survey of advances in vision-based human motion capture and analysis," *Comput. Vis. Image Understanding*, vol. 104, pp. 90–126, 2006.

[19] A. De Santis, B. Siciliano, A. De Luca, and A. Bicchi, "An atlas of human-robot interaction," *Mech. Mach. Theory*, vol. 43, pp. 253–270, 2008.

[20] J. Versace, "A review of the severity index," in *Proc. 15th Stapp Car Crash Conf.*, 1971, pp. 771–796.

[21] K. Salisbury, W. Townsend, B. Ebrman, and D. DiPietro, "Preliminary design of a whole-arm manipulation system (WAMS)," in *Proc. IEEE Int. Conf. Robot. Autom.*, 1988, vol. 1, pp. 254–260.

[22] G. Hirzinger, J. Bals, M. Otter, and J. Stelter, "The DLR-KUKA success story: Robotics research improves industrial robots," *IEEE Robot. Automat. Mag.*, vol. 12, no. 3, pp. 16–23, Sep. 2005.

[23] M. Zinn, O. Khatib, and B. Roth, "A new actuation approach for human friendly robot design," in *Proc. IEEE Int. Conf. Robot. Autom.*, 2004, vol. 1, pp. 249–254.

[24] G. Pratt and M. Williamson, "Series elastic actuators," in *Proc. IEEE/RSJ Int. Conf. Intell. Robot. Syst.*, 1995, vol. 1, pp. 399–406.

[25] K. Kong, J. Bae, and M. Tomizuka, "Control of rotary series elastic actuator for ideal force-mode actuation in human-robot interaction applications," *IEEE/ASME Trans. Mechatronics*, vol. 14, no. 1, pp. 105–118, Feb. 2009.

[26] G. Tonietti, R. Schiavi, and A. Bicchi, "Design and control of a variable stiffness actuator for safe and fast physical human/robot interaction," in *Proc. IEEE Int. Conf. Robot. Autom.*, 2005, pp. 526–531.

[27] C.-M. Chew, G.-S. Hong, and W. Zhou, "Series damper actuator: a novel force/torque control actuator," in *Proc. 4th IEEE/RAS Int. Conf. Humanoid Robot.*, 2004, vol. 2, pp. 533–546.

[28] A. Bicchi, G. Tonietti, and R. Schiavi, "Safe and fast actuators for machines interacting with humans," in *Proc. 1st IEEE Tech. Exhib. Based Conf. Robot. Autom. TExCRA 2004*, pp. 17–18.

[29] R. W. Phillips, "Engineering applications of fluids with a variable yield stress," Ph.D. dissertation, Univ. California, Berkeley, CA, 1969.

[30] J. Carlson and B. Spencer Jr., "Magneto-rheological fluid dampers for semi-active seismic control," in *Proc. 3rd Int. Conf. Motion Vibration Control*, 1996, vol. 3, pp. 35–40.

[31] N. Takesue, J. Furusho, and Y. Kiyota, "Fast response MR-fluid actuator," *J. Soc. Mech. Eng. Int. J. Ser. C*, vol. 47, no. 3, pp. 783–791, 2004.

[32] Lord Corporation. (2008, Jul.). "MR-132DG Magneto-Rheological Fluid," Lord Tech. Data, rev. 1, [Online]. Available: http://www.lordfulfillment.com/upload/DS7015.pdf

[33] R. S.-R. Daniela Susan-Resiga and L. Vékás, "A rheological model for magneto-rheological fluids," in *Proc. 3rd Ger. Romanian Workshop Turbomach. Hydrodyn.*, 2007, pp. 141–158. Q7

[34] M. Sakaguchi and J. Furusho, "Development of high-performance actuators using er fluids," *J. Intell. Mater. Syst. Struct.*, vol. 10, no. 8, pp. 666–670, 1999.

Alex S. Shafer was born in Haifa, Israel. He received the B.E.Sc. and the M.E.Sc. degrees in electrical and computer engineering from the University of Western Ontario, London, ON, Canada, in 2006 and 2009, respectively, where he is currently working toward the Ph.D. degree.

He is the cofounder of Innovent Designs, where he has been an Electronics Design Consultant since 2007. In 2009, he was awarded a Mitacs Accelerate internship to develop a multi-DOF magneto-rheological-based robot. In 2010, he joined QDAC Inc., where he is an Electronics Engineer. His research interests include optimization and design of human-friendly actuation systems. Q8

Mehrdad R. Kermani (M'xx) received the Ph.D. degree in electrical and computer engineering from the University of Western Ontario, London, ON, Canada, in 2005.

From 1997 to 2001, he was a Senior Automation Consultant in the field of the steel industry. He is currently an Assistant Professor in the Department of Electrical and Computer Engineering, University of Western Ontario, and a Senior Scientist at the Canadian Surgical Technologies and Advanced Robotics (CSTAR) Research Centre, London Health Sciences Centre, London, ON. His research interests include human-safe robotic systems, smart materials, and actuation. Q9

QUERIES

Q1: Author: The affiliation of author M. R. Kermani has been modified according to the information provided in the biography. Please check if OK.

Q2. Author: Please check if edit done to sentence " MR fluids can produce maximum yield stresses. . ." is OK.

Q3. Author: Please check if the edit done to sentence "A fair comparison would dictate" is OK.

Q4. Author: Please specify whether the previous section in the sentence "In the previous section. . ." refers to Section IV. If not, please provide the specific section number.

Q5. Author: Figures 12 and 13 have been renumbered. Please check if OK.

Q6. Author: PLease check if Ref. [4] is OK as typeset and also provide the publisher and location.

Q7. Author: Please check if Ref. [33] is OK as typeset.

Q8. Author: Please provide complete mailing address and also to be included in affiliation

Q9. Author: Please provide the year in which M. R. Kermani became the member of IEEE.

On the Feasibility and Suitability of MR Fluid Clutches in Human-Friendly Manipulators

Alex S. Shafer and Mehrdad R. Kermani, *Member, IEEE*

***Abstract*—An investigation into the suitability of magneto-rheological (MR) clutches in the context of developing feasible actuation solutions for physical human–robot interaction is presented. Contact and collision forces pose great danger to humans, and thus, the primary criteria for actuator development is safety. While the majority of existing solutions make use of mechanical compliance in some form, in this paper, we will approach the problem by considering the use of MR clutches for coupling the motor drive to the joint. The suitability of MR actuators to provide an intrinsically safe actuation platform is investigated by modeling the torque to mass, and torque to inertia ratios, as well as output impedance of the MR clutch. These figures are compared to commercially available servo motors as well as mechanically compliant based human-safe actuator models. The MR clutch is analytically shown to have superior mass and inertia characteristics over servo motors while either matching or surpassing the intrinsic safety characteristics of the modeled compliant actuator. The implementation of MR-clutch-based actuation systems is investigated by examining the distributed active semiactive approach. The proposed approach is discussed in terms of mechanical as well controller complexity and relates the investigation to the feasibility of practical implementations. Performance characteristics are empirically investigated by experimentation with a prototype MR clutch constructed for this purpose. The prototype MR clutch can transmit torque up to 75 Nm and has a bandwidth of 30 Hz. Torque to mass and torque to inertia ratios of the prototype MR clutch are substantially greater than that of comparable servo motors. Conclusions drawn from this investigation indicate that indeed MR clutch actuation approaches can be developed to balance safety and performance while maintaining reasonable system complexity.**

***Index Terms*—Human–robot interaction, magneto-rheological (MR) fluids, safety and performance.**

I. Introduction

INCREASINGLY, we are witnessing a growing number of developments in the field of robotics characterized by their intent to integrate man and machine in a safe and functional manner [1]–[3]. The suitability of a manipulator to work in close proximity with humans is determined first by the level of safety it can guarantee toward its human counterparts. Guaranteeing safety is a difficult if not impossible exercise as we can rarely guarantee the dependability of the numerous components required to complete a modern manipulator. Add in the human factor, and our task becomes insurmountable. Thus, much focus has been centered on interactive robots that are expected to perform in a safe and dependable manner in unknown and unpredictable environments. Collisions between robots and humans constitute the primary safety concern. Such collisions are responsible for numerous injuries each year [4], despite the existence of barriers and other fail-safe mechanisms. As we move closer toward a shared environment, new approaches to manipulator design are becoming increasingly important. Devices utilizing the unique properties of magneto-rheological (MR) fluids have been developed for robotic applications, however, almost entirely for use in haptic systems [5]–[9]. While it has been suggested in the literature how such devices might be used in a manipulator to improve both safety and performance (i.e., [10], [11]), there appears to be a general reluctance toward adopting such technology as a viable alternative to the current solutions.

Control design and software issues for the manipulators intended to interact with humans also present a set of unique challenges [12]. It is necessary to address safety, not only at the design, but at motion planning and control levels as well. Of high importance are identification and assessment of various sources of danger [13]–[16] as well as obtaining simple but realistic models of the environment and in particular of humans [17], [18]. It is however, beyond the scope of this paper to adequately discuss all subject matters. For more comprehensive review of the software issues see [19].

This paper is organized in seven sections. Section II briefly discusses fundamental issues relating to actuator and manipulator design that have detrimental effects on safety, as well as review the shortcomings of existing solutions. Section III reviews the construction and principles of the MR clutch, used to develop MR actuators (MRAs). Section IV presents an investigation into MR clutch actuators' figures of merit to provide a comparison to differing actuator types. In Section V, we propose an elaborated MR-based actuation approach that leverages the strengths highlighted in the previous section. The goals of the proposed actuation approach are to maintain safe physical interactions with humans, while improving the performance over existing human-safe actuation techniques. Section VI highlights the results of performance validation experiments conducted on a prototype MRA. Finally, concluding remarks are given in Section VII.

Manuscript received March 24, 2010; revised July 2, 2010; accepted July 17, 2010. Recommended by Technical Editor M. O'Malley.

A. S. Shafer is with the Department of Electrical and Computer Engineering, University of Western Ontario, London, ON N6A 5B9, Canada (e-mail: ashafer2@uwo.ca).

M. R. Kermani is with the Department of Electrical and Computer Engineering, University of Western Ontario, London, ON N6A 5B9, Canada, and also with the Canadian Surgical Technologies and Advanced Robotics (CSTAR) Research Centre, London Health Sciences Centre, London, ON N6A 5A5, Canada. (e-mail: mkermani@eng.uwo.ca).

Q1

Color versions of one or more of the figures in this paper are available online at http://ieeexplore.ieee.org.

Digital Object Identifier 10.1109/TMECH.2010.2074210

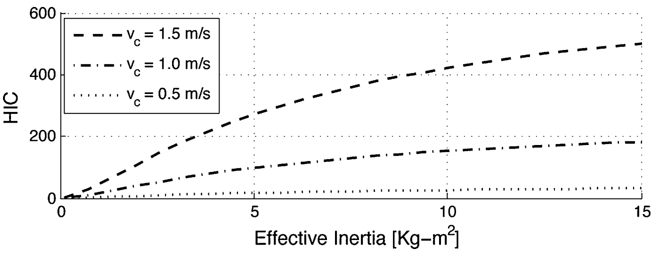

Fig. 1. Simulated HIC of a single-axis manipulator. The simulated link is rigidly coupled to the input drive. Here, V_c is collision velocity.

II. Human-Friendly Manipulators: Background and Analysis

In attempts to guarantee the safety of humans within a shared workspace, much research has been focused on the development of manipulators which are intrinsically safe. That is, manipulators which by means of their mechanical properties can guarantee some level of collision safety in the absence of a controller. To understand the degree of safety one might associate with a manipulator, we may look at the results of an uncontrolled collision through the use of the head injury criterion (HIC) [20]. The HIC along with its variations have long been used by the automotive industry to gauge the severity of collisions. In the field of robotics, it can also be used to gain similar insight. The HIC is defined as

$$\mathrm{HIC} = \max_{t_1, t_2} \left\{ (t_2 - t_1) \left(\frac{1}{t_2 - t_1} \int_{t_1}^{t_2} a(t) dt \right)^{2.5} \right\} \qquad (1)$$

where a is the acceleration of the head (in g's), and t_1 and t_2 are times within the collision selected to maximize the HIC, such that $t_1 < t_2$. An HIC of 100 is the maximum value considered to be nonlife threatening. To gauge how the effective inertia of a link is related to a manipulator's inherent ability to collide safely, we simulate a single-axis robot colliding with a human head (see Fig. 1). As we may have expected, the results of the HIC indicate that a manipulator's safety can be improved by reducing its effective inertia. Thus, a generation of light-weight manipulators was inspired. One of the first manipulators to be designed under the light-weight paradigm was the whole arm manipulator (WAM) [21]. The WAM uses steel cable transmission allowing actuators to be located at the manipulator's base. Another successful implementation is the DLR-III [22]. Using light-weight carbon composites to form its links as well as advanced actuator design integrated with low-weight harmonic reduction gears, allows the DLR-III to attain a fully integrated light-weight design. These approaches however address only half of the problem. Robotic manipulators make use of high-performance servo motors to drive their links. These servo motors produce low output torque, and at high velocity with respect to what is suitable for most robots. To remedy this, gear-reduction systems are most commonly employed. The resulting torque at the link is the actuator torque multiplied by the gear ratio G_r, while the reflected actuator inertia associated with the rotor of the motor is multiplied by G_r^2. Thus, the effective inertia experienced by a robotic link can be expressed as

$$J_e = J_\ell + G_r^2 J_r \qquad (2)$$

where J_ℓ is the inertia of the link, and J_r is the rotor inertia of the motor. The reflected actuator inertia of a manipulator can in fact be much larger than that of the link [23], thereby contributing a larger share of the inertial load during collisions. In response to this, several novel actuation systems have been proposed which work to decouple the reflected actuator inertia from the link. Receiving considerable attention are actuation systems that introduce compliance into their transmission. series elastic actuator (SEA) [24] accomplishes precisely this by integrating an elastic element between the motor and link. Intuitively, lower coupling stiffness results in collisions producing lower HIC values. The addition of the elastic element however dramatically reduces the controllable bandwidth of the actuator [25]. The integration of SEA devices establish a trade-off between safety and performance as a function of coupling stiffness. The variable stiffness actuator (VSA) [26] was developed to address the stringent safety-performance trade-off characterized by the SEA. Like the SEA, the VSA incorporates an elastic element into its transmission. The VSA however can alter the stiffness of the transmission coupling during task execution. It can be observed from Fig. 1 that at lower velocities, collisions involving stiff manipulators may still occur safely. By dynamically varying the stiffness to be compliant for high velocities, and stiff at low velocities, performance can be improved while maintaining safety.

Chew *et al.* [27] proposed the series damper actuator (SDA) as a means of achieving force/torque control. The SDA is constructed by placing a rotary damper in series with the motor drive. Force/torque control is achieved by controlling the relative angular velocity between the motor drive and the damper output. Similar to the SEA, the SDA has inherent impact absorption properties, which are attributed to the dissipative nature of the series damper. Similarly to the addition of an elastic element, the SDA reduces the actuator bandwidth for decreasing coupling viscosity. Again, a trade-off exists between safety and performance, in this case parameterized by the damping coefficient. (It should be noted that the authors of [27] suggest how MR fluids can be used to vary the damping coefficient). Using a damping element over an elastic element subsequently reduces the order of the system by one. This implies that the SDA is capable of achieving a larger force bandwidth over the SEA.

Variable impedance actuation (VIA) [28] combines both variable elastic and variable damping elements in the transmission. This approach is an extension of the VSA concept. By being able to vary both an elastic and a damping element, it is possible to again recuperate performance during task execution while guaranteeing the safety of humans. The VIA further requires additional actuators to vary coupling parameters.

Another notable variation on the SEA is the distributed macro-mini actuation approach (DM^2) [23]. Actuation of the joint is achieved by the coupling of a low-frequency high-torque SEA with a high-frequency low-torque servo. The high-frequency servo, directly coupled to the joint, is used to actuate the manipulator in a complimentary frequency space to that of the

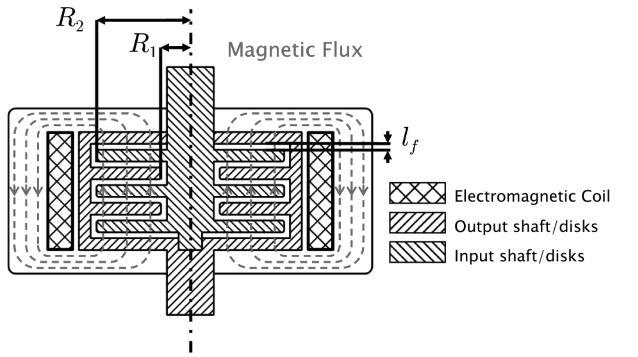

Fig. 2. Cross section of a multidisk style MR clutch and its corresponding magnetic circuit.

SEA. In this way, the effective controllable bandwidth of the manipulator is improved. The low-torque high-frequency servo is selected such that its output inertia is minimized. Thus, safety is maintained while performance is improved.

III. MR Clutch

MR fluids are a suspension of micrometer-sized particles in a carrier fluid. When subjected to a magnetic field, the particles aggregate into columns aligned in the direction of the field. Subsequently, the columns act to resist shearing of the fluid perpendicular to the field. The apparent yield stress of the fluid is dependant on, and increases with the intensity of the applied field.

Fig. 2 is a cross section of a multidisk style MR fluid clutch. MR fluid fills the volume between input and output disks. Rotation of the input shaft causes shearing in the fluid with respect to the output shaft. By energizing the electromagnetic coil, a field is induced in the MR fluid altering its apparent viscosity. The outer casing of the MR clutch acts as the magnetic flux path required to complete the magnetic circuit. The Bingham viscoplastic model is commonly used to represent the shear stress of the fluid as a function of the applied field and shear rate [29]. The model is given by

$$\tau = \tau_y(\mathbf{H}) + \eta\frac{dv}{dz}, \qquad \tau > \tau_y \tag{3}$$

where τ is the shear stress, τ_y is the field-dependant yield stress, $\mathbf{H}$ is the applied magnetic field intensity, η is the newtonian viscosity, and dv/dz is the velocity gradient in the direction of the field. Applying the Bingham viscoplastic model to a clutch, we define r as the radius from the rotational axis, and l_f as the thickness of the fluid-filled gap between input and output disks. In situations where $r \gg l_f$ for $r \in [R_1, R_2]$ (see to Fig. 2), the velocity gradient becomes constant. We can then rewrite (3) as

$$\tau = \tau_y(\mathbf{H}) + \eta\dot{\gamma}(r), \qquad \tau > \tau_y \tag{4}$$

where the shear rate $\dot{\gamma}$ is defined as

$$\dot{\gamma} = \frac{\omega r}{l_f} \tag{5}$$

and ω is the angular velocity between input and output shafts of the clutch. The torque produced by a circumferential element at a radius r is given by

$$dT = 2\pi r^2 \tau dr. \tag{6}$$

We define a clutch as having N output disks. Substituting (4) into (6) and integrating across both faces of each output disk, we arrive at

$$\begin{aligned} T &= 2N\int_{R_1}^{R_2} 2\pi\left(\tau_y(\mathbf{H})r^2 + \eta\frac{\omega r^3}{l_f}\right) dr \\ &= 4N\pi\left(\frac{\tau_y(\mathbf{H})(R_2^3 - R_1^3)}{3} + \frac{\eta\omega(R_2^4 - R_1^4)}{4l_f}\right) \end{aligned} \tag{7}$$

as the torque transmitted by an N-disk clutch. Data relating the yield stress τ_y of a fluid to an applied field are generally published by the manufacturer. The viscosity η of the carrier fluid is typically in the range of 0.1–0.3 Pas. The maximum torque transmission capability of an MR clutch is dependent on the maximum yield stress the material can produce. MR fluids exhibit saturation in their yield stress at high field strengths. This is a result of the underlying physics, and limits the amount of torque a particular MR fluid can transmit in clutch applications. MR fluids can produce maximum yield stresses typically in the range of 50–100 kPa [30] depending on their chemistry. MR fluids respond to an applied field on the order of 1 ms. However, the actuation response of an MR clutch becomes delayed due to field propagation through the magnetic circuit [31]. Q2

IV. MR Clutch Actuators: Investigating Figures of Merit

In Section II, we discussed the effects of actuator mass, output inertia, and output impedance on safety. In this section, we will present models relating torque to mass, torque to inertia, as well as the output impedance of (MRA).

Several configurations exist in which MR clutches can be utilized to develop an actuation system. The simplest configuration utilizes a motor to drive an MR clutch, which in turn drives the joint. To generalize the discussion, we will consider simplified mechanical models of the MR clutch based on the model presented in Section III. Note that in this section, we define the actuator output to be the output of an MR clutch.

A. Actuator Inertia

MRAs have the characteristic of replacing the reflected rotor inertia of the motor with the reflected inertia of the clutch output shaft and disks. The benefit of MRAs is their high torque to output inertia ratio as compared to servo motors. To show this, we approximate the radius of the output shaft to be equivalent to R_1. The moment of inertia of a single output disk, J_d is given by

$$J_d = \frac{1}{2}\pi\rho_d l_d\left(R_2^4 - R_1^4\right) \tag{8}$$

where ρ_d is the mass density of the disk material, l_d is the thickness of the disk (commonly between 0.5 to 1 mm), and R_1 and R_2 define the minor and major radii, respectively, of the output disk. If we consider the torque transmitted solely by the field-dependant yield stress of the MR fluid, the torque transmission of a single disk is then given by

$$T_d = \frac{4}{3}\pi\tau_y\left(R_2^3 - R_1^3\right). \tag{9}$$

Furthermore, if we consider R_1 to be small, i.e., $R_2 \gg R_1$, then the contribution of the shaft region to both (8) and (9) is also small. By allowing R_1 to equal zero, we can approximate the torque–inertia ratio of a single disk to be

$$\alpha = \frac{T_d}{J_d} = \frac{8}{3}\frac{\tau_y}{\rho_d l_d R_2}. \tag{10}$$

As observed, the ratio becomes less favorable as R_2 increases. This however is not the final measure that dictates the actuators suitability. To grasp the overall effects of increasing radius, and hence, torque capacity, the reflected inertia at the joint should be consider. The reason for this is that as radius increases along with torque capacity, the gear ratio required to amplify the actuator's torque decreases. As the actuator inertia multiplies the square of the gear ratio to arrive at the reflected inertia at the joint, the analysis becomes important. The reflected inertia of the MR clutch at the manipulator joint is given by

$$J_c' = \frac{1}{2}\pi\rho_d l_d N\left(R_2^4 - R_1^4\right)G_r^2 \tag{11}$$

where we have included N to multiply the inertia by the number of disks in the clutch. The gear ratio G_r is defined as

$$G_r = \frac{T_c'}{T_c} \tag{12}$$

where T_c' is the desired torque at the joint, and T_c is the output torque of the clutch. Rearranging (9) to show the outer radius R_2 as a function of the clutch output torque yields

$$R_2 = \left(\frac{3}{4}\frac{T_c}{\pi\tau_y N} + R_1^3\right)^{1/3}. \tag{13}$$

We can then write (13) representing the reflected inertia of a MR clutch at the manipulator joint as a function of the clutch torque

$$J_c' = \frac{1}{2}\pi\rho_d l_d N\left(\left(\frac{3}{4}\frac{T_c}{\pi\tau_y N} + R_1^3\right)^{4/3} - R_1^4\right)\left(\frac{T_c'}{T_c}\right)^2. \tag{14}$$

Fig. 3 shows the values of reflected actuator inertia versus output torque for the MR clutch. The plot also includes equivalent values for commercially available low-inertia servo motors. It is evident that the MR clutch demonstrates superior output inertia characteristics over the low-inertia servo motors. We note that the developed torque to inertia relationship improves dramatically at larger values of output torque.

B. Mass of MR Clutch

In this section, we develop torque to mass relationships for the MR clutch. While the relationships are developed using simplified geometric models, they serve to establish the order in which the clutch mass compares to that of servo motors, as well as the rate at which clutch mass increases with respect to transmittable torque capacity. To develop a relationship between clutch mass

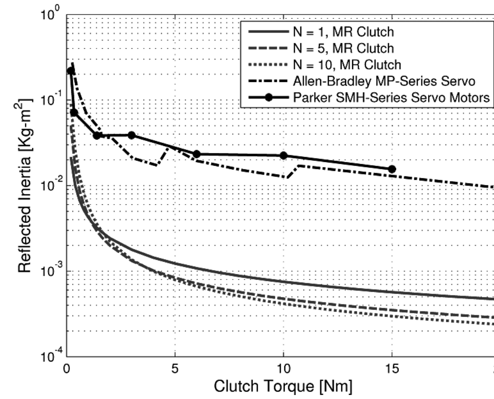

Fig. 3. Reflected inertia versus output torque for the MR clutch (see Table I) and commercially available low-inertia servo motors. ($T_c' = 50$ Nm).

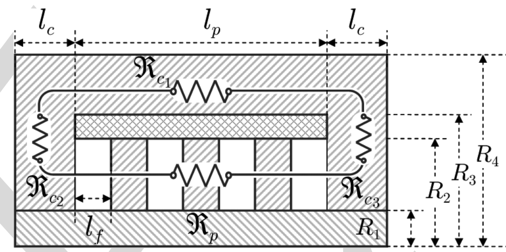

Fig. 4. Simplified MR clutch model. The electromagnetic coil is contained between R_2 and R_3, and R_4 defines the outer surface of the ferrous core.

and torque capacity for MR fluid clutches, we consider the simplified geometric model detailed in Fig. 4. We will solve for required parametric values through the application of magnetic circuit analysis. We divide the reluctance of the core $\Re_c$ into three sections, namely $\Re_{c_1}$, $\Re_{c_2}$, and $\Re_{c_3}$. The symmetric geometry of the model dictates the reluctance $\Re_{c_2}$ to be equivalent to that of $\Re_{c_3}$. Thus, we define the reluctance of the core to be

$$\Re_c = \Re_{c_1} + 2\,\Re_{c_{23}} \tag{15}$$

where $\Re_{c_{23}} = \Re_{c_2} = \Re_{c_3}$. We have defined a clutch by the number of output disks N coupled to the output shaft. For N output disks, a clutch is required to have $N - 1$ input disks, and a total of $2N$ MR fluid interface gaps positioned between input and output disks. In the simplified model of Fig. 4, we define both geometric and material properties of the input and output disks to be identical. The disk pack assembly thus contains $2N - 1$ disks and $2N$ MR fluid interface gaps. The reluctance of the disk pack assembly $\Re_p$ can then be written as

$$\Re_p = (2N - 1)\,\Re_d + 2N\,\Re_f \tag{16}$$

where $\Re_d$ and $\Re_f$ are the reluctance of a single disk and single MR fluid interface gap, respectively. The reluctance of a material is given by $\Re = l/(\mu_0\mu_r A)$, where l is the mean length of the flux path through the material, $\mu_0 = 4\pi \times 10^{-7}$ H/m is the permeability of free space, μ_r is the relative permeability of the material, and A is the cross-sectional area of the material perpendicular to the flux path. Assuming that the mean flux path through any of the circuit members lies at its geometric center,

TABLE I
PARAMETER VALUES FOR SIMPLIFIED MR CLUTCH MODEL

Parameter	Symbol	Value
Disk thickness	l_d	1.0 [mm]
Fluid gap thickness	l_f	0.5 [mm]
Disk minor radius	R_1	10 [mm]
Max operating yield stress	τ_y^*	40 [kpa]
Coil current density	J_w	2.5 $\times 10^6$ [A/m^2]

we can then derive the reluctance of the individual components of the simplified clutch model to be

$$\Re_{c_1} = \frac{l_p + l_c}{\mu_0 \mu_{r_s}\, \pi \left(R_4^2 - R_3^2\right)}$$
$$\Re_{c_{23}} = \int_{R_2 + R_1/2}^{R_4 + R_3/2} \frac{dr}{\mu_0 \mu_{r_s}\, (2\pi r)\, l_c} = \frac{\ln\left(R_4 + R_3/R_2 + R_1\right)}{2\mu_0 \mu_{r_s}\, \pi l_c}$$
$$\Re_d = \frac{l_d}{\mu_0 \mu_{r_s}\, \pi \left(R_2^2 - R_1^2\right)} \quad \Re_f = \frac{l_f}{\mu_0 \mu_{r_f}\, \pi \left(R_2^2 - R_1^2\right)}. \quad (17)$$

Here, μ_{r_s} is the permeability of steel, the material used for both the core and disks, μ_{r_f} is the permeability of the MR fluid, l_d is the thickness of a single disk, l_f is the distance between input and output disks forming the MR fluid gap, l_c is the thickness of the equivalent core sections, and $l_p = (2N - 1)\, l_d + 2Nl_f$ is the length of the disk pack. The flux ϕ in the circuit is then given by

$$\phi = \frac{I}{\Re_c + \Re_p} = \frac{l_p (R_3 - R_2) J_w}{\Re_c + \Re_p} \quad (18)$$

where I is the total electric current through the cross section of the magnetic coil, and J_w is the current density of the coil cross section. The magnetic field intensity $\mathbf{H}$ at any point within the circuit is related to the circuit flux ϕ by

$$\mathbf{H} = \frac{\phi}{\mu_0 \mu_r A} \quad (19)$$

where again, μ_r and A are, respectively, the relative permeability and cross sectional area of the material at which the magnetic-field intensity $\mathbf{H}$ is to be determined. We now define the parameter τ_y^* as the maximum yield stress at which the MR fluid is to operate. Using data provided by the MR fluid manufacturer relating the yield stress of the fluid to the applied magnetic field, we define $\mathbf{H}^*$ as the magnetic-field intensity in the MR fluid required to produce the yield stress τ_y^*. Rearranging (19), and substituting the appropriate MR fluid geometric and material values, we define ϕ^* as the flux required in the circuit to produce $\mathbf{H}^*$ in the MR fluid

$$\phi^* = \mu_0 \mu_{r_f}\, \pi \left(R_2^2 - R_1^2\right)\, \mathbf{H}^*. \quad (20)$$

R_2 is uniquely defined by the parameters T_c, N, R_1, and τ_y^* [refer to (13)]. Thus, for the given set of fixed parameters given in Table I, we solve for the values of R_3, R_4, and l_c that satisfy (18) for $\phi = \phi^*$, while simultaneously minimizing the clutch mass m_{MRC} given by

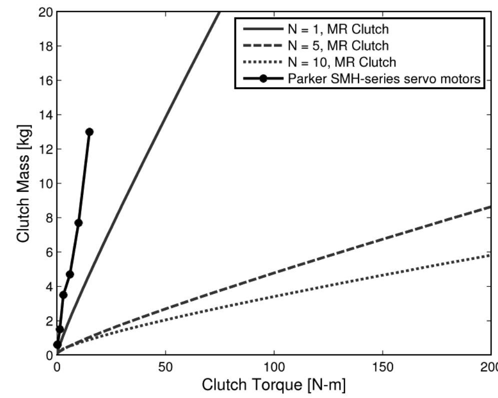

Fig. 5. Mass of simplified clutch models versus torque capacity (calculated using MR fluid characteristics of Lord Corp., MR-132DG MR fluid [32]).

$$\begin{aligned} m_{\text{MRC}} &= m_c + m_p + m_s + m_w \\ m_c &= \pi \left[\left(R_4^2 - R_3^2\right) l_p + 2\left(R_4^2 - R_1^2\right) l_c\right] \rho_s \\ m_p &= \pi \left[(2N - 1)\, l_d \rho_s + 2N l_f \rho_f\right] \left(R_2^2 - R_1^2\right) \\ m_w &= \pi \left(R_3^2 - R_2^2\right) l_p \rho_{\text{cu}} \qquad m_s = \pi R_1^2 \left(l_p + 2\, l_c\right) \rho_{\text{al}} \end{aligned} \quad (21)$$

where m_c is the mass of the core, m_p is the mass of the disk pack assembly which includes the MR fluid, m_s is the mass of the shaft, and m_w is the mass of the magnetic coil. In (21), ρ_s, ρ_f, ρ_{cu}, and ρ_{al} are the mass densities of steel, MR fluid, copper, and aluminum, respectively. Fig. 5 shows the torque to mass relationship of the simplified MR clutch model and compares it to a commercially available servo motor. We note that due to the mass overhead associated with the material required to form the magnetic circuit, the torque to mass ratio of the MR clutch is less favorable at very low values N. In the developed model, we observe superior characteristics over the commercially available servo motor.

C. Output Impedance

The output impedance of an actuator can be defined as

$$Z(s) = \frac{F_l(s)}{X_l(s)} \quad (22)$$

where $F_l(s)$ is the force experienced by the load and $X_l(s)$ is the displacement of the load. Actuators that limit or reduce their impedance, especially at higher frequencies, offer a higher degree of safety over those that do not. Within the controllable bandwidth, impedance can be actively reduced by control action. However, above the controllable bandwidth, the impedance is dominated by the open-loop characteristics of the actuator and link. To form a comparison of the intrinsic properties of human safe actuators, we consider the output impedance in the absence of control. This is intended to represent the open-loop characteristics resulting from collisions occurring above the control bandwidth. Fig. 6 shows a schematic representation of the MRA and SEA models under consideration here. In this scenario, both

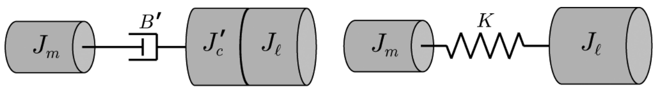

Fig. 6. Model schematic of unpowered (a) MRA, and (b) SEA.

motor and clutch are unpowered, allowing us to model the clutch as a damper and inertial load. J_m is the inertia of the motor for both the MRA and SEA, K is the spring constant of the SEA, B'_c is the damping coefficient of the MR clutch reflected to the link, J'_c is the output inertia of the MR clutch reflected to the link, and J_ℓ is the inertia of the link. The damping coefficient in the MR clutch is determined by the Newtonian viscosity of the MR fluid (the viscosity at zero field) as well as the clutch geometry. The output impedance of the SEA is given by

$$Z_{\text{SEA}} = J_\ell s^2 + \frac{K J_m s^2}{J_m s^2 + K}. \tag{23}$$

The value of the link inertia J_ℓ for the purpose of discussing the characteristics of the SEA is somewhat arbitrary, and it is, thus, not uncommon to disregard it (allowing J_ℓ to equal zero). This results in the properties of the SEA being characterized by the second term only. In this circumstance, the output impedance approaches the value of the spring constant K at high frequencies. It is this property of the SEA to limit output impedance above the controllable bandwidth that intrinsically insures safe interaction forces as well as impact loads. The output impedance of the MRA is given as

$$Z_{\text{MRA}} = (J'_c + J_\ell)\, s^2 + \frac{B'_c J_m s^2}{J_m s + B'_c}. \tag{24}$$

A fair comparison would dictate if we once more disregard the link inertia J_ℓ. While the second term increases (approximately) proportional to the reflected damping coefficient B'_c, at higher frequencies it is the reflected inertia of the clutch J'_c in the first term that dominates the dynamics of the output impedance. Noting that the output impedance of the MRA is not limited, but rather continues to grow at high frequencies, seemingly, it would not appear that the MRA poses the intrinsic safety characteristics of the SEA. However, to fairly evaluate the deficiency of the MRA in this respect, it is instructive to consider practical examples to establish the context in which the SEA offers superior safety. If we reconsider the actuator models to include the inertia of the link, for both the SEA and MRA, the inertial impedance represented in the first terms will dominate the output impedances at higher frequencies. The output impedance of the MRA can thus approach that of the SEA if $J'_c \ll J_\ell$. To demonstrate the conditions in which we can satisfy $J'_c \ll J_\ell$, we consider an applications requiring 50 Nm at the link. From the values presented in Fig. 3, we can expect that the reflected inertia of an MRA satisfying the 50-Nm requirement, would be on the order of 10^{-3} kg m^2. We may then prescribe a lower bound link inertia on the order of $J_\ell = 10^{-2}$ kg m^2, and one order of magnitude larger than J'_c, the result of which being that $(J_\ell + J'_c) \approx J_\ell$. To put the values into perspective, we can express this lower bound as a link modeled by a point mass of 250 g at a radius of 20 cm. Links having inertias above this lower bound could then be driven by either MRA or SEA and exhibit nearly identical inertial impedances. In the application region of 50 Nm, it is reasonable to expect that most links will have inertias larger than our defined lower bound. The implication being that an SEA would not provide a safety improvement over an MRA in the stated application region. It must be pointed out that we have assumed the values presented in Fig. 3, which have been computed from idealized models, are realistically achievable. Fig. 7 shows simulated output impedances for both an MRA and SEA. Values for the motor, MR clutch, and link inertias, as well as clutch damping coefficient were obtained from an experimental MRA setup (discussed later in greater detail). Using these values, the output impedance of the MRA is simulated and compared to that of an SEA. We see that in this circumstance, the MRA demonstrates superior output impedance characteristics over that of the SEA. This is complimented by the superior performance provided by the MRA.

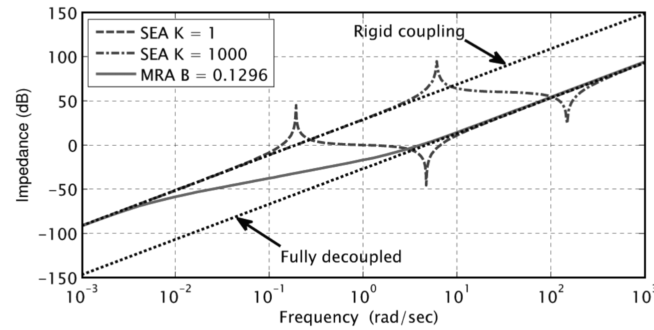

Fig. 7. Simulated output impedance for SEA and MRA. Values obtained from experimental MRA setup: $J_m = 26.9$ kg m^2; $J'_c = 5 \times 10^{-3}$ kg m^2; $J_\ell = 0.045$ kg m^2; $B = 0.1296$ Ns m^{-1}. MRA produces 75-Nm output.

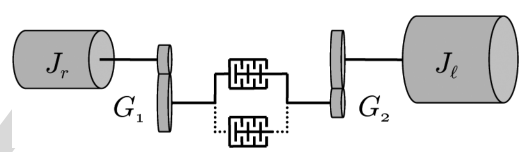

Fig. 8. DASA: solid line represents single clutch configuration, dotted line represents connection to second clutch present only in antagonistic configuration.

V. Distributed Active SemiActive Actuation

In this section, we propose an actuation technique that leverages the unique properties of MRAs. The proposed technique is unique in which we attempt to reconcile safety, performance, and complexity into a feasible solution. The distributed active semiactive (DASA) actuation approach locates a driving motor (the active actuator) at the base of the robot, and a semiactive MR clutch at the joint (see to Fig. 8). The gear ratios G_1 and G_2 are balanced to give the desired mass, and reflected output inertia at the link. Reducing G_1 reduces the requirements of the clutch transmission torque, which thus reduces the mass of the clutch, however, the reflected output inertia is inevitably increased as G_2 must then be increased to compensate. In Section IV, we have shown how actuating a joint via an MR clutch can reduce mass and reflected output inertia over conventional servo motors. The impact on safety is immediately appreciated as the effective inertia of the link is instantly reduced. This not only improves manipulator performance, but further allows a manipulator to operate at higher velocities while maintaining safe HIC values in the event of a collision. Moreover, the clutch itself is back drivable, and can be thought of as exhibiting the properties of an ideal torque source. This is an important characteristic for human-friendly actuators as it facilitates impedance control. While motors themselves are also intrinsically back drivable, the high-ratio-gear reductions they require are often not. Thus, highly performing low-weight robots, which implement low mass motors at the expense of high-ratio-gear reductions rely on torque sensors in the control loop to electronically implement back-drivable behavior. MR clutches posses a superior torque to mass ratios over their servo motor counterparts, and thus can be designed to require much lower reduction ratios, if not developed as direct-drive components, either way retaining their intrinsic back-drivability. MR clutches have the added benefit of uniform torque transmission independent of armature position, unlike servo motors, which suffer from nonlinearities such as cogging torque. Relocating the driving motor to the base of a robot in order to reduce the mass at the link is not a new concept. However, it has been a restrictive practice as the newly required transmission responsible for bringing mechanical power from the base to the joint has commonly introduced unwanted friction and compliance, which have reduced performance, and complicated the control system. The DASA implementation however can be controlled to operate in a region in which torque transmission is relatively immune to perturbation in the relative angular velocity ω within the clutch, effectively allowing the clutch to act as a mechanical power filter. This characteristic which will be explained momentarily allows the DASA system to function with less than ideal mechanical transmission while maintaining the performance and characteristics of a "stiff" transmission at the joint. To explain this, we consider that the the Bingham model is accurate for describing the rheology of the fluid for shear stress τ above the field-dependant yield stress τ_y, as expressed in (3). It is this "Bingham region" in which we wish the clutch to operate in order to benefit from the aforementioned characteristics. Below the yield stress τ_y, however, the fluid exhibits newtonian characteristics, i.e., to say that τ grows with a nonnegligible proportionality to the shear rate $\dot{\gamma}$ (for a more in-depth analysis see [33]). We can thus attribute a field-dependant shear rate threshold $\dot{\gamma}^*$ below, which the fluid exhibits newtonian characteristics, and above which, the Bingham model applies. To maintain the clutch in the Bingham region, the fluid at any radius r within the clutch must maintain a shear rate above $\dot{\gamma}^*$. To guarantee this condition, we define the field-dependant angular velocity ω^*, the threshold above which operation in the Bingham region is ensured as

$$\omega^* = \frac{\dot{\gamma}^* l_f}{R_1}. \tag{25}$$

We come to (25) by rearranging (5) and substituting r with its minimum value R_1, the critical radius at which the lowest shear rate $\dot{\gamma}$ occurs. The control strategy should therefore attempt to avoid entering the Newtonian region by controlling the motor angular velocity ω_m to satisfy the condition

$$|\omega_m| = |\omega_j - \omega^*| + \epsilon^* \tag{26}$$

where ω_j is the angular velocity of the joint, and ϵ^* is a field-dependant error margin selected to ensure that the dynamics of the motor have enough time to react to quickly varying values of ω_j. ϵ^* must be large enough to ensure $\omega \geq \omega^*$ under all dynamic situations, however, exact calculation of ϵ^* may be difficult as there is a reliance on empirical data associated with the dynamics of the joint/link. Care must be taken, however, to avoid unnecessary power dissipation, which for a clutch is defined as $P_d = T\omega$. Because ω tracks $\omega^* + \epsilon^*$, the value selected for ϵ^* cannot be arbitrarily large. Crossing into the Newtonian region is required to alter the direction of the torque transmitted to the link when utilizing a single clutch to implement the DASA system. As the motor must change the direction of its output rotation, the clutch torque transmission momentarily enters a dead zone. This has the potential of creating a substantial backlash effect.

A. Antagonistic DASA

An antagonistic configuration of the DASA system (see Fig. 8) is intended to increase performance, and rectify the shortcomings of the single-clutch DASA configuration. The motor drives the input to two clutches, however in opposite directions with respect to one another. The antagonistic output of the two clutches is coupled to the link. By energizing one of the two clutches, torque can be transmitted in either the clockwise or counterclockwise direction. Thus, the antagonistic configuration allows for torque transmission to the joint to alter direction without altering the direction of the motor output, thereby, eliminating the backlash introduced by the single-clutch DASA. Such devices have been developed with electro-rheological (ER) fluids [34]. Maintaining rotation of the motor shaft, the bandwidth of the antagonistic-DASA output is limited by charging and discharging of the magnetic field required to activate the clutch. If we label the two clutches of an antagonistic DASA assembly as $\mathcal{C}_1$ and $\mathcal{C}_2$, then the motor's angular velocity should track

$$\omega_m = \max\{|\omega_j - \omega_1^*|, |\omega_2^* - \omega_j|\} + \epsilon^* \tag{27}$$

to avoid entering the Newtonian region of operation in either clutch. ω_1^*, and ω_2^* are the angular velocity of the Bingham region thresholds for clutches $\mathcal{C}_1$ and $\mathcal{C}_2$, respectively. Note that in our convention, clutch $\mathcal{C}_2$ has its input reversed in direction with respect to clutch $\mathcal{C}_1$, i.e.,

$$\omega_1 = \omega_j - \omega_m \qquad \omega_2 = \omega_j + \omega_m. \tag{28}$$

The torque production for an antagonistic-DASA system operating in the Bingham region is then given by

$$T_{\mathrm{AD}} = T_1(\mathbf{H}_1) + T_2(\mathbf{H_2}) - \frac{2\pi\eta|\omega_j|}{l_f}\left(R_2^4 - R_1^4\right) \tag{29}$$

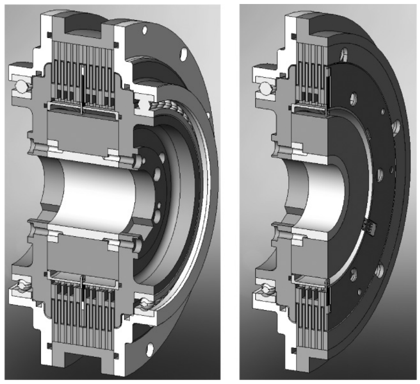

Fig. 9. Sectional views of prototype MR clutch.

where T_1 and T_2 are the field-dependant torques produced by clutches $\mathcal{C}_1$, and $\mathcal{C}_2$, respectively, given by

$$T_i = \frac{4\pi}{3}\tau_y(\mathbf{H}_i)\left(R_2^3 - R_1^3\right)\operatorname{sgn}(\omega_i), \quad i = 1, 2 \qquad (30)$$

where $\mathbf{H}_1$ and $\mathbf{H}_2$ are the fields produced in clutches $\mathcal{C}_1$, and $\mathcal{C}_2$, respectively. Note that the individual viscous torque contributions of $\mathcal{C}_1$ and $\mathcal{C}_2$ negate each other at the joint when $\omega_j = 0$. Viscosity of this class of fluids does not always obey ideal models. The antagonistic configuration can mitigate some nonlinearities which would otherwise have to be compensated for by the controller.

VI. Performance Validation of a Prototype MR Clutch

In this section, we present results obtained by experimentation with a prototype MR clutch which we have designed and constructed (see Fig. 9). The configuration of the prototype MR clutch deviates from the model of Section IV. The magnetic coil of the prototype is located radially inward of the clutch pack in a "coil-in" configuration, as opposed to the coil-out configuration previously discussed. Coupling the coil to the output shaft has the intended effect of reducing clutch mass, however comes at the expense of increasing output inertia. Design of the prototype clutch is partially automated using the optimization process discussed in Section IV-B, where model equations have been updated to reflect the change in configuration. The method returns values for the dimensional parameters that minimize the clutch mass for a given design torque. The prototype MR clutch was specified with a design torque of 120 Nm. The dimensional parameters returned by the optimization process were used as the basis for practical design. Table II compares the output torque, inertia, and mass of the physical prototype MR clutch to the optimized design model. A large discrepancy exists between the modeled and actual torque. The discrepancy results primarily due to deviations in the physical design from the geometric model used in the optimization. Practical design features required for fastening and wire access are omitted from the model. The optimization produces geometries in which flux members enter magnetic saturation at the magnitude of circuit flux corresponding to the specified design torque of the clutch. Removal of ferromagnetic material from the optimized geometry subsequently results in premature saturation of the circuit, limiting the output torque of the clutch.

TABLE II
Comparison Between Prototype and Modeled MR Clutch, as Well as Commercially Available Servomotors

	Coil-out Configuration	Prototype MR Clutch Model	Prototype MR Clutch Actual	Servomotors Parker SMH-100	Servomotors Maxon EC60
Output Torque[Nm]	75	120	75	6.0	0.83
Mass[kg]	2.8	4.7	4.5	4.7	2.5
Inertia$\times 10^3$[kg$\cdot$m^2]	0.19	2.8	5.0	0.34	0.083
Reflected Inertia$\times 10^3$[kg$\cdot$m^2]†	-	-	2.22	23.3	302

†Reflected torque $T_c' = 50$ Nm.

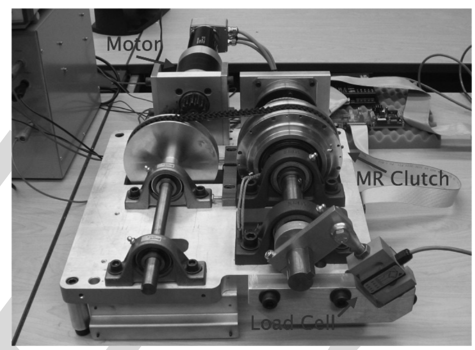

Fig. 10. Experimental setup used to verify the prototype MR clutch.

Much of our analysis prior to this section is based on the coil-out configuration model of Section IV-B. To add perspective, we compare this model to the prototype MR clutch. The values for the coil-out configuration shown in Table II are produced with the geometric model and procedure described in Section IV-B, where the output torque is specified to match the constructed MR clutch and not the design value. The coil-out model does not consider any practical design requirements, such as bearings, seals, and mechanical coupling of the disks. In this regard, the model represents an ideal scenario, or baseline for the achievable characteristics in its configuration. The comparison indicates that there is room for improvement of the prototype MR clutch. Ideally, mass could be reduced by a third, while the output inertia might be improved by an order of magnitude. Table II compares the prototype MR clutch to two commercially available servo motors. The servo motors are chosen to have comparable mass to the prototype MR clutch. The output inertia of the servo motors are between one and two orders of magnitude lower than that of the MR clutch. However, when we consider a hypothetical application requiring a 50-Nm output, the prototype MR clutch posses the more favorable reflected inertia by at least an order of magnitude.

To assess its performance characteristics, the clutch is mounted to an experimentation platform (see Fig. 10) that incorporates an angular encoder (Renishaw RM22I) to read the position of the output shaft. A static load cell (Transducer Techniques SBO-1K) mounts to the output shaft for torque experiments. A servo motor (Maxon EC 60) provides the rotational input to the MR clutch. A PID controller is implemented on a

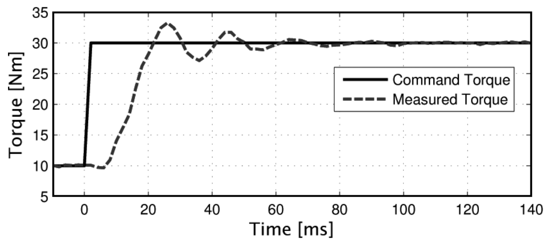

Fig. 11. Torque tracking of step reference.

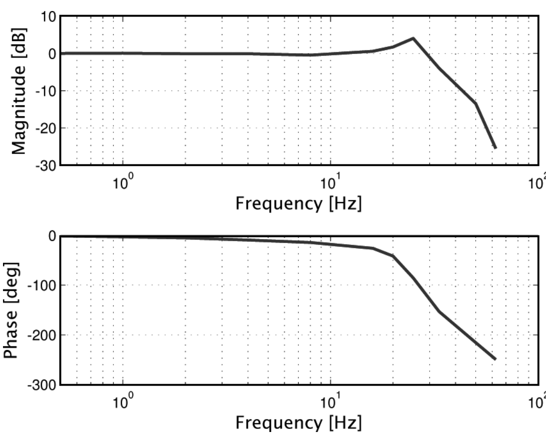

Fig. 12. Frequency response of the prototype MR clutch.

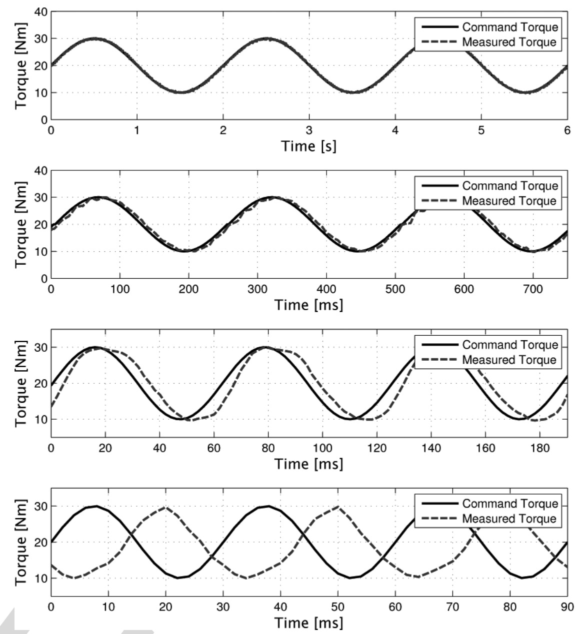

Fig. 13. Torque tracking of a sinusoidal references at frequencies of 0.5, 4.0, 16.0, and 33.3 Hz (from top to bottom).

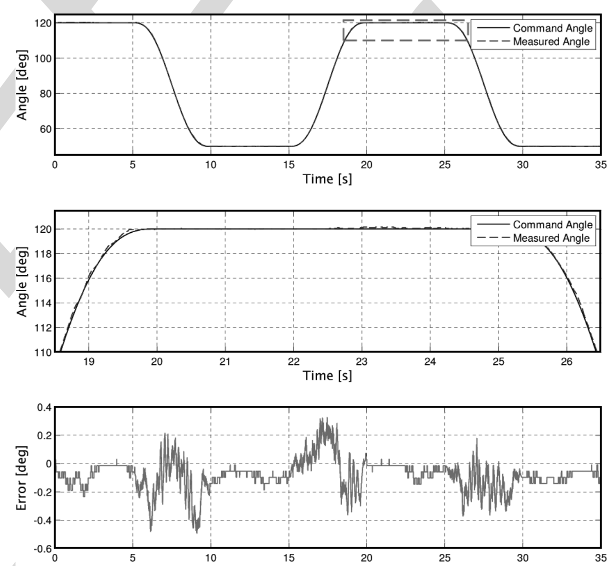

Fig. 14. Position tracking of a trajectory reference. The center plot magnifies the trajectory in the region marked by the dotted red bounding box.

desktop computer that communicates with the experimentation platform via a National Instruments (NI USB-6229) multifunction I/O device. The output signal from the PID controller forms the input signal to the current amplifier of the MR clutch, while the rotational velocity of the motor is kept constant.

Fig. 11 shows the closed-loop response to a step input. The rise time is determined to be approximately 10 ms. The frequency response and dynamic characteristics are examined by measuring the torque response to a sinusoidal reference signal and initiating a frequency sweep at 0.5 Hz. Fig. 12 shows the frequency response of the system. The resulting 3-dB actuator bandwidth is measured to be approximately 30 Hz. Fig. 13 presents a set of four time domain measurements from the sweep. Beginning at 0.5 Hz, we note excellent overlay of the measured signal with that of the command. As the reference frequency is increased toward and above the actuator bandwidth, we note that the response remains very smooth and as well retains the shape of the command signal quite well. Clean and predictable torque outputs are an asset to the development of controls and sensorization schemes that are required to monitor and control contact forces between manipulators and humans.

Trajectory tracking experiments were conducted using the angular encoder to form the feedback signal. The motor output was held at a constant rotational velocity. A 50-cm long arm constructed of medium density plastic was coupled to the output shaft. A counter weight of approximately 2 kg was mounted to the end of arm. The results shown in Fig. 14 indicate the capacity of the MR clutch in this arrangement to achieve favorable precision in position control tasks. Small fluctuation errors in the static portions of the trajectory demonstrate the capability of the MR clutch to suppress fluctuations present in the input drive.

VII. Conclusion

MR fluids exhibit promising characteristics for applications in robotics. Specifically, they are well-suited for actuation systems developed to interact physically with humans. As we have shown, MR-clutch-based actuators demonstrate excellent torque to mass, and torque to inertia characteristics. This is especially evident for clutches having large torque capacities. This creates a niche opportunity for MR-based actuators to be developed into light-weight direct-drive (DD) systems. Light-weight

DD systems exhibit several characteristics that are sought after for human-friendly manipulators, namely: intrinsic backdrivability, low output inertia, superior performance and bandwidth, as well as high precision in the control of output torque. Furthermore, MR-based actuators can potentially reduce system complexity. Potentially, the accuracy of torque transmission models in such systems could allow for high fidelity torque control without the requirement for torque sensors at the joints. This is in contrast to the increasingly complex actuation solutions proposed to deal with physical human interaction.

References

[1] G. Hirzinger, "Mechatronics for a new robot generation," *IEEE/ASME Trans. Mechatronics*, vol. 1, no. 2, pp. 149–157, Jun. 1996.

[2] Y. Yamada, Y. Hirasawa, S. Huang, Y. Umetani, and K. Suita, "Human-robot contact in the safeguarding space," *IEEE/ASME Trans. Mechatronics*, vol. 2, no. 4, pp. 230–236, Dec. 1997.

[3] H. Lim and K. Tanie, "Collision-tolerant control of human-friendly robot with viscoelastic trunk," *IEEE/ASME Trans. Mechatronics*, vol. 4, no. 4, pp. 417–427, Dec. 1999.

[4] Industrial Robots and Robot System Safety in *OSHA Technical Manual*, United States Department of Labor, Occupational Safety and Health Administration, 2008, ch. 4. Q6

[5] J. Blake and H. B. Gurocak, "Haptic glove with mr brakes for virtual reality," *IEEE/ASME Trans. Mechatronics*, vol. 14, no. 5, pp. 606–615, Oct. 2009.

[6] Y.-J. Nam and M.-K. Park, "A hybrid haptic device for wide-ranged force reflection and improved transparency," in *Proc. Int. Conf. Control, Autom. Syst.*, 2007, pp. 1015–1020.

[7] D. Ryu, K. Moon, S. Kang, M. Kim, and J.-B. Song, "Development of wearable haptic system for tangible studio to experience a virtual heritage alive," in *Proc. IEEE/RSJ Int. Conf. Intell. Robots. Syst.*, 2006, pp. 466–471.

[8] T. Kikuchi, K. Oda, and J. Furusho, "Simulation of clonic movement with leg-robot driven by compact mr fluid clutch," in *Proc. IEEE 11th Int. Conf. Rehabil. Robot.*, 2009, pp. 80–85.

[9] S. H. Winter and M. Bouzit, "Use of magnetorheological fluid in a force feedback glove," *IEEE Trans. Neural Syst. Rehabil. Eng.*, vol. 15, no. 1, pp. 2–8, Mar. 2007.

[10] P. Fauteux, M. Lauria, M.-A. Legault, B. Heintz, and F. Michaud, "Dual differential rheological actuator for robotic interaction tasks," in *Proc. IEEE/ASME Int. Conf. Adv. Intell. Mechatron.*, 2009, pp. 47–52.

[11] S.-S. Yoon, S. Kang, S.-J. Kim, Y.-H. Kim, M. Kim, and C.-W. Lee, "Safe arm with mr-based passive compliant joints and visco-elastic covering for service robot applications," in *Proc. IEEE/RSJ Int. Conf. Intell. Robots. Syst.*, 2003, pp. 2191–2196.

[12] J. Trafton, N. Cassimatis, M. Bugajska, and D. Brock, "Enabling effective human-robot interaction using perspective-taking in robots," *IEEE Trans. Syst. Man Cybern.*, vol. 35, no. 4, pp. 460–470, Jul. 2005.

[13] K. Ikuta and M. Nokata, "Safety evaluation method of design and control of human-care robots," *Int. J. Robot. Res.*, vol. 22, pp. 281–297, 2003.

[14] O. Brock and O. Khatib, "Elastic strips: A framework for motion generation in human environments," *Int. J. Robot. Res.*, vol. 21, pp. 1031–1053, 2002.

[15] D. Kulic and E. Croft, "Pre-collision safety strategies for human-robot interaction," *Auton. Robots*, vol. 22, pp. 149–164, 2007.

[16] N. Najmaei and M. Kermani, "Prediction-based reactive control strategy for human-robot interactions," in *Proc. IEEE Int. Conf. Robot. Autom.*, 2010, pp. 3434–3439.

[17] A. Martinez and J. Vitria, "Clustering in image space for place recognition and visual annotations for human-robot interaction," *IEEE Trans. Syst. Man Cybern.*, vol. 31, no. 5, pp. 669–682, Oct. 2001.

[18] T. Moeslund, A. Hilton, and V. Kruger, "A survey of advances in vision-based human motion capture and analysis," *Comput. Vis. Image Understanding*, vol. 104, pp. 90–126, 2006.

[19] A. De Santis, B. Siciliano, A. De Luca, and A. Bicchi, "An atlas of human-robot interaction," *Mech. Mach. Theory*, vol. 43, pp. 253–270, 2008.

[20] J. Versace, "A review of the severity index," in *Proc. 15th Stapp Car Crash Conf.*, 1971, pp. 771–796.

[21] K. Salisbury, W. Townsend, B. Ebrman, and D. DiPietro, "Preliminary design of a whole-arm manipulation system (WAMS)," in *Proc. IEEE Int. Conf. Robot. Autom.*, 1988, vol. 1, pp. 254–260.

[22] G. Hirzinger, J. Bals, M. Otter, and J. Stelter, "The DLR-KUKA success story: Robotics research improves industrial robots," *IEEE Robot. Automat. Mag.*, vol. 12, no. 3, pp. 16–23, Sep. 2005.

[23] M. Zinn, O. Khatib, and B. Roth, "A new actuation approach for human friendly robot design," in *Proc. IEEE Int. Conf. Robot. Autom.*, 2004, vol. 1, pp. 249–254.

[24] G. Pratt and M. Williamson, "Series elastic actuators," in *Proc. IEEE/RSJ Int. Conf. Intell. Robot. Syst.*, 1995, vol. 1, pp. 399–406.

[25] K. Kong, J. Bae, and M. Tomizuka, "Control of rotary series elastic actuator for ideal force-mode actuation in human-robot interaction applications," *IEEE/ASME Trans. Mechatronics*, vol. 14, no. 1, pp. 105–118, Feb. 2009.

[26] G. Tonietti, R. Schiavi, and A. Bicchi, "Design and control of a variable stiffness actuator for safe and fast physical human/robot interaction," in *Proc. IEEE Int. Conf. Robot. Autom.*, 2005, pp. 526–531.

[27] C.-M. Chew, G.-S. Hong, and W. Zhou, "Series damper actuator: a novel force/torque control actuator," in *Proc. 4th IEEE/RAS Int. Conf. Humanoid Robot.*, 2004, vol. 2, pp. 533–546.

[28] A. Bicchi, G. Tonietti, and R. Schiavi, "Safe and fast actuators for machines interacting with humans," in *Proc. 1st IEEE Tech. Exhib. Based Conf. Robot. Autom. TExCRA 2004*, pp. 17–18.

[29] R. W. Phillips, "Engineering applications of fluids with a variable yield stress," Ph.D. dissertation, Univ. California, Berkeley, CA, 1969.

[30] J. Carlson and B. Spencer Jr., "Magneto-rheological fluid dampers for semi-active seismic control," in *Proc. 3rd Int. Conf. Motion Vibration Control*, 1996, vol. 3, pp. 35–40.

[31] N. Takesue, J. Furusho, and Y. Kiyota, "Fast response MR-fluid actuator," *J. Soc. Mech. Eng. Int. J. Ser. C*, vol. 47, no. 3, pp. 783–791, 2004.

[32] Lord Corporation. (2008, Jul.). "MR-132DG Magneto-Rheological Fluid," Lord Tech. Data, rev. 1, [Online]. Available: http://www.lordfulfillment.com/upload/DS7015.pdf

[33] R. S.-R. Daniela Susan-Resiga and L. Vékás, "A rheological model for magneto-rheological fluids," in *Proc. 3rd Ger. Romanian Workshop Turbomach. Hydrodyn.*, 2007, pp. 141–158. Q7

[34] M. Sakaguchi and J. Furusho, "Development of high-performance actuators using er fluids," *J. Intell. Mater. Syst. Struct.*, vol. 10, no. 8, pp. 666–670, 1999.

Alex S. Shafer was born in Haifa, Israel. He received the B.E.Sc. and the M.E.Sc. degrees in electrical and computer engineering from the University of Western Ontario, London, ON, Canada, in 2006 and 2009, respectively, where he is currently working toward the Ph.D. degree.

He is the cofounder of Innovent Designs, where he has been an Electronics Design Consultant since 2007. In 2009, he was awarded a Mitacs Accelerate internship to develop a multi-DOF magneto-rheological-based robot. In 2010, he joined QDAC Inc., where he is an Electronics Engineer. His research interests include optimization and design of human-friendly actuation systems. Q8

Mehrdad R. Kermani (M'xx) received the Ph.D. degree in electrical and computer engineering from the University of Western Ontario, London, ON, Canada, in 2005.

From 1997 to 2001, he was a Senior Automation Consultant in the field of the steel industry. He is currently an Assistant Professor in the Department of Electrical and Computer Engineering, University of Western Ontario, and a Senior Scientist at the Canadian Surgical Technologies and Advanced Robotics (CSTAR) Research Centre, London Health Sciences Centre, London, ON. His research interests include human-safe robotic systems, smart materials, and actuation. Q9

QUERIES

Q1: Author: The affiliation of author M. R. Kermani has been modified according to the information provided in the biography. Please check if OK.
Q2. Author: Please check if edit done to sentence " MR fluids can produce maximum yield stresses. . ." is OK.
Q3. Author: Please check if the edit done to sentence "A fair comparison would dictate" is OK.
Q4. Author: Please specify whether the previous section in the sentence "In the previous section. . ." refers to Section IV. If not, please provide the specific section number.
Q5. Author: Figures 12 and 13 have been renumbered. Please check if OK.
Q6. Author: PLease check if Ref. [4] is OK as typeset and also provide the publisher and location.
Q7. Author: Please check if Ref. [33] is OK as typeset.
Q8. Author: Please provide complete mailing address and also to be included in affiliation
Q9. Author: Please provide the year in which M. R. Kermani became the member of IEEE.